




On depositional processes governing along-strike facies variations of fine-grained deposits: Unlocking the Little Ice Age subaqueous clinothems on the Adriatic shelf

CLAUDIO PELLEGRINI* , IRENE SAMMARTINO*, JUERGEN SCHIEBER† ,
TOMMASO TESI‡, FRANCESCO PALADINI DE MENDOZA§, VERONICA ROSSI¶,
JACOPO CHIGGIATO§, KATRIN SCHROEDER§, ANDREA GALLERANI*,
LEONARDO LANGONE‡, FABIO TRINCARDI** and ALESSANDRO AMOROSI¶ 

*Istituto di Scienze Marine (ISMAR-CNR), Via Gobetti 101, Bologna 40129, Italy (E-mail: claudio.pellegrini@bo.ismar.cnr.it)

†Department of Geological Sciences, Indiana University, East 10th Street, Bloomington 1001, IN, USA

‡Istituto di Scienze Polari (ISP-CNR), Via Gobetti 101, Bologna 40129, Italy

§Istituto di Scienze Marine (ISMAR-CNR), Arsenale Tesa 104, Castello, Venezia 2737/F, Italy

¶Department of Biological, Geological and Environmental Sciences, University of Bologna, Via Zamboni 67, Bologna 40126, Italy

**Dipartimento di Scienze del Sistema Terra e Tecnologie per l'Ambiente, CNR, Piazzale Aldo Moro 7, Roma 00185, Italy

Associate Editor – Kevin Taylor

ABSTRACT

Depositional processes recorded by shelf deposits may vary widely along-strike, depending largely on the mode of delivery and deposition of sediments to the basin. In fine-grained systems in particular, depositional processes are difficult to reconstruct with standard facies analysis of sediment cores due to the ostensibly featureless and homogenous appearance of muds. In this study, sedimentological, palaeontological, geochemical, and oceanographic data were combined in a detailed characterization of depositional conditions via sedimentary structures, type of organic matter, trace-metal geochemistry, and benthic fauna assemblages (foraminifera and ostracods) along the 600 km long shelf delta clinothems of the West Adriatic shelf (Italy). Processes inferred from sedimentary facies and micro-structures were then considered in the context of the modern Adriatic oceanographic regime. Specific attention was given to the Little Ice Age stratigraphic unit (1500–1850 CE), which contains a continuum of genetically related fine-grained strata. The Little Ice Age deposit offers the opportunity to examine a source-to-sink system with the high resolution typical of modern analogues, at a time interval when Apennine rivers were not yet hydraulically engineered with man-made sediment traps along their trunks. Individual beds within the Little Ice Age muddy prodelta form hectometre to kilometre-wide bedsets that reflect the interplay between energetic meteo-ocean conditions (storm-dominated beds), flood supply (river-dominated beds or hyperpycnites) and along-shelf bottom-current dispersion (drift-dominated beds). The multidisciplinary approach applied at different scales of observations helped in understanding sediment provenance and the relative timing of sediment transport before final burial that strongly promoted organic matter oxygen exposure and the loss of carbon by microbial degradation. Overall, the distinctive depositional processes that acted in concert along the prodelta slope produced a subtle lateral heterogeneity of preserved sedimentary structures, faunal associations, and organic matter composition in a laterally-continuous

lithostratigraphic unit deposited at centennial scale. These findings have implications on the forcing conditions that ultimately control the location and nature of fine-grained beds in both modern and ancient, mud-dominated depositional systems.

Keywords Along-strike facies variations, depositional processes, Late-Holocene, palaeo-flood occurrence, river delta, sediment archive.

INTRODUCTION

Fine-grained sedimentary rocks (grain size $<62.5\ \mu\text{m}$; Lazar *et al.*, 2015a,b), commonly known as shales or mudstones, constitute about two-thirds of the sedimentary rock record (Schieber, 1998; Schieber *et al.*, 2000; Potter *et al.*, 2012), thus representing the bulk of recorded geological history (Schieber, 1998; Li *et al.*, 2015); a key record also to assess climate and environmental variability through geological time (e.g. Hedges *et al.*, 1997; Oldfield *et al.*, 2003; Blair *et al.*, 2004; Berner *et al.*, 2007; Piva *et al.*, 2008; Boulesteix *et al.*, 2019; Hage *et al.*, 2022). Recent studies of marine mudstones (Schieber *et al.*, 2007; Macquaker *et al.*, 2010; Schieber, 2011, 2016; Laycock *et al.*, 2017; Li & Schieber, 2018; Li *et al.*, 2021) show that these rocks may consist of coarse silt to sand-sized, mud-dominated composite particles (composed of multiple clay or silt-size mineral grains). Thus, transport and deposition of muds is likely to be subject to more complex processes than commonly appreciated (Palinkas & Nittrouer, 2006; Wheatcroft *et al.*, 2006; Goni *et al.*, 2008; Bhattacharya & MacEachern, 2009; Macquaker *et al.*, 2010; Bohacs *et al.*, 2014; Plint, 2014; Walsh *et al.*, 2014; Wilson & Schieber, 2014; Li *et al.*, 2015; Pellegrini *et al.*, 2015, 2021; Lazar *et al.*, 2015b; Bao *et al.*, 2016; Schieber, 2016; Birgenheier *et al.*, 2017; Collins *et al.*, 2017; Laycock *et al.*, 2017; Boulesteix *et al.*, 2019; Schieber *et al.*, 2019; Bhattacharya *et al.*, 2020; Paz *et al.*, 2022). Because fine-grained sediments preserve information about past conditions, mud and mudstones are key archives that need to be interpreted accurately, taking into consideration the variability of sediment supply and the suite of post-depositional processes. Tracking sediment from source to final resting place (Source-to-Sink; S2S) is considered essential for trying to connect adjacent segments of the sediment routing system to infer palaeo-environmental controls on sedimentation patterns and to improve understanding of particle transfer from

land to the ocean (e.g. Goodbred *et al.*, 2003; Sømme *et al.*, 2011; Bohacs *et al.*, 2014; Amorosi *et al.*, 2016, 2022; Bentley *et al.*, 2016; Bhattacharya *et al.*, 2020). Key drivers in fine-grained depositional systems include even subtle variations in sediment supply and oceanographic regime. It is difficult, however, to obtain a firm grip on key depositional processes, because of the (in most cases) poor temporal resolution of sedimentary packages, the difficulty in deciphering sediment catchment characteristics, and the complexity of sediment dispersal pathways (e.g. Mellere *et al.*, 2002; Mutti *et al.*, 2003; Morris *et al.*, 2006; Jerolmack & Paola, 2010; Petter, 2010; Poyatos-Moré *et al.*, 2016; Pellegrini *et al.*, 2020; Hage *et al.*, 2022; Anell *et al.*, 2023).

Most mud shelf deposits are mixed-process systems that have been influenced by rivers, waves, tides and currents to varying degrees at the same time (Nittrouer *et al.*, 1986; Bentley & Nittrouer, 2003; Goodbred *et al.*, 2003; Liu *et al.*, 2006; Bhattacharya & MacEachern, 2009; Jaramillo *et al.*, 2009; Macquaker *et al.*, 2010; Ainsworth *et al.*, 2011; Patruno & Helland-Hansen, 2018; Peng *et al.*, 2022). The degree by which these processes influence deposition within a muddy shelf deposit complex changes laterally, along-dip as well as along-strike. In addition, prodelta deposits may be less reworked/eroded by fair-weather waves, compared to shallower, and more energetic environments (for example, sandy delta-front deposits), and thus the prodelta facies has the potential to contain an almost complete record of river floods and oceanographic events. Primary formative processes of thin-bedded prodelta deposits include surge-type turbidity currents, hyperpycnal flows, and storm-driven waves and bottom currents (Stow & Shanmugam, 1980; Normark & Piper, 1991; Mulder & Syvitski, 1995; Myrow *et al.*, 2002, 2008; Mulder *et al.*, 2003; Friedrichs & Scully, 2007; Lamb *et al.*, 2008; Talling *et al.*, 2012; Plint, 2014).

Several recent studies have been conducted to investigate variations in depositional processes in deltaic systems by examining prodelta deposits along depositional dip. Based on the detailed

facies analysis of event beds from prodelta units of the Minturn Formation, Lamb *et al.* (2008) illustrated variations in the relative influence of turbidity currents and storm surges from proximal to distal settings. These studies suggest that the variability of the mud-dominated prodelta facies may directly reflect the dominant sediment delivery process (Schieber, 1998; Lamb *et al.*, 2008; Myrow *et al.*, 2008; Macquaker *et al.*, 2010). However, only a few studies of modern mud shelf deposits have analyzed thin-bedded prodelta facies in detail to evaluate along-strike variations in depositional processes (Walsh & Nittrouer, 2009; Li *et al.*, 2015; Denommee *et al.*, 2018).

At first glance, mudstones appear quite homogenous (Schieber, 1999; Bhattacharya & MacEachern, 2009; Plint, 2014), because in outcrop they show: (i) a high degree of weathering that can preclude detailed analysis; and (ii) uncertainties regarding the linkage between sedimentary fabrics and flow characteristics of primary formative processes (i.e. surge-type turbidity currents, hyperpycnal flows, storm surges, bottom current transport of flocculated muds), as well as potential interactions between turbidity currents and other types of bottom currents (Mulder *et al.*, 2008; Fonnesu & Felletti, 2019; Miramontes *et al.*, 2020; Pellegrini *et al.*, 2021). One added challenge in the analysis of modern muds is their typically high initial water content, which requires time-consuming techniques to turn 'soup' and 'toothpaste' into something that can be put under the microscope (e.g. Walsh & Nittrouer, 2009; Schieber, 2011; Potter *et al.*, 2012; Denommee *et al.*, 2018; Pellegrini *et al.*, 2021).

The Late-Holocene Highstand Systems Tract of the Western Adriatic shelf attains a thickness of 35 m and includes prodelta clinothems that were deposited during the Little Ice Age (LIA), with sediment accumulation rates locally reaching >2 cm/yr (Correggiari *et al.*, 2005; Cattaneo *et al.*, 2007; Piva *et al.*, 2008). These clinothems reflect the influence of coalescing Alpine and Apennine rivers and prograde on the continental shelf (Fig. 1; Cattaneo *et al.*, 2003; Harris *et al.*, 2008; Palinkas, 2009; Traykovski *et al.*, 2007; Pellegrini *et al.*, 2015, 2021).

This study examines the LIA fine-grained unit in three sectors of the Adriatic shelf, where along-strike facies variations were governed by distinct depositional processes. The study focuses on small-scale sedimentary features that have not been previously described and extracts the main

processes that drove sediment deposition along the prodelta slope (*sensu* Patruno *et al.*, 2015; Patruno & Helland-Hansen, 2018; Pellegrini *et al.*, 2020). An integrated approach is used herein that combines palaeontological (benthic foraminifera and ostracods) and geochemical (terrestrial biomarkers and trace element distribution) data with observations across a wide range of stratigraphic and sedimentological scales (from kilometres to microns). The LIA interval offers a unique opportunity to examine the lateral heterogeneity of a muddy unit deposited in only 350 years with high sediment accumulation rates (up to 2.3 cm/yr) and extending over >600 km along the shelf. This unit, which accumulated in a pristine environment well before dam construction in the contributing drainages, includes the record of high-frequency storm events that are related to the notable climatic deterioration associated with the Little Ice Age. The LIA prodelta clinothems on the Adriatic shelf can be considered as a modern analogue for predicting along-strike facies variations in ancient shales: a natural laboratory where boundary conditions (for example, sediment provenance, distance from the river mouth, basin physiography, oceanographic regime and climatic conditions) are firmly established and where sediment dispersal processes can be chronologically constrained. This study demonstrates that different depositional processes are recorded fragmentarily even along a hundreds of kilometres long muddy unit, formed within decadal to centennial scales. However, under optimal preservation conditions, prodelta beds offer a high-fidelity record of river flood events that may be useful for the reconstruction of frequency and intensity of past precipitation.

BACKGROUND

The Little Ice Age

The Little Ice Age was a climatic oscillation dated back to *ca* 1500–1850 CE (Matthes, 1939; Bradley & Jonest, 1993), which affected the whole Northern Hemisphere (Bond *et al.*, 1997, 2001; Campbell *et al.*, 1998; McDermott *et al.*, 2001; Fig. 2). Although the forcing mechanisms of the LIA are still under debate (e.g. Crowley, 2000; Foukal *et al.*, 2004; Jones & Mann, 2004), a decrease in temperatures and an increase in precipitation were reported all over Europe (Büntgen *et al.*, 2011; Jalali *et al.*, 2018) and are

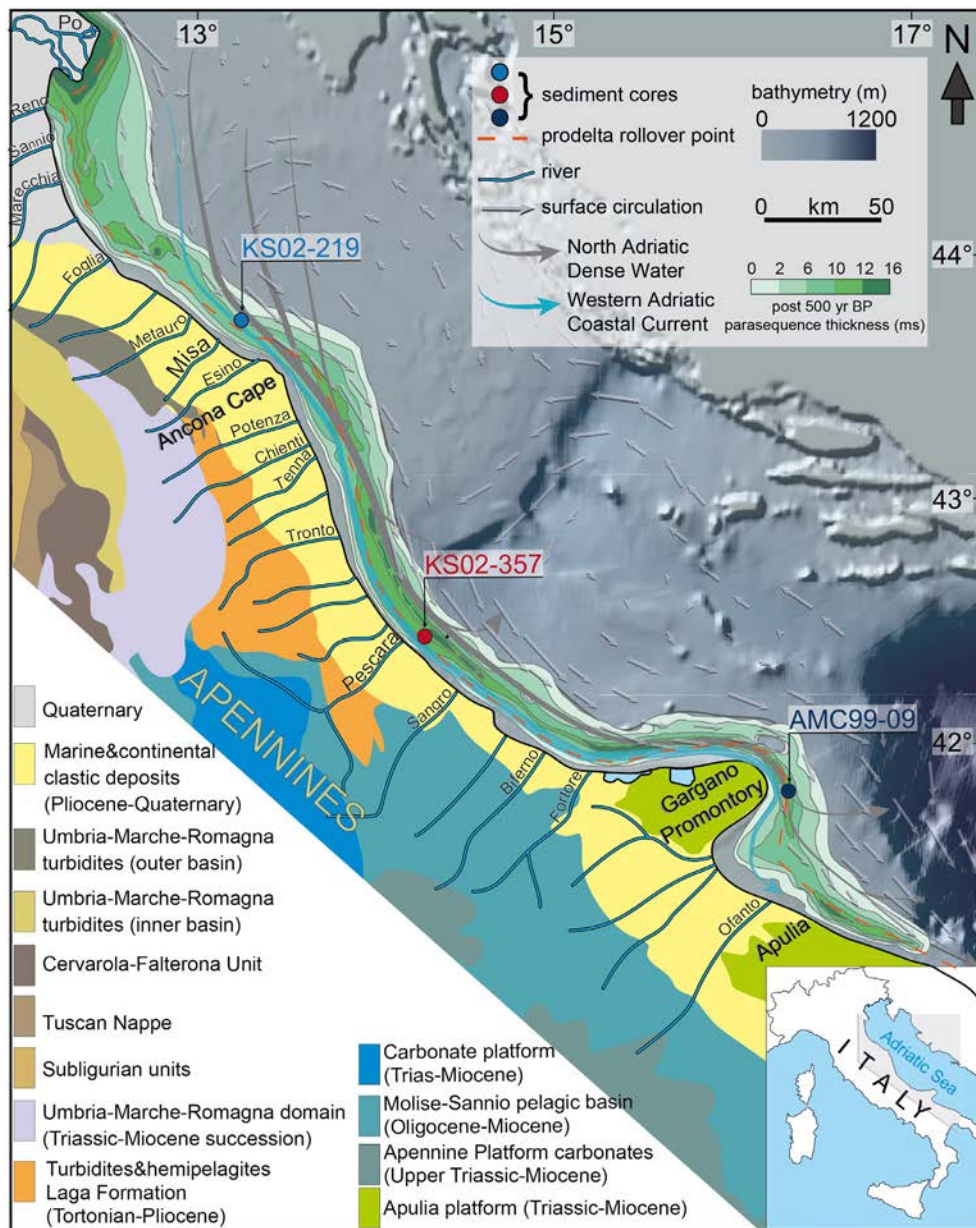


Fig. 1. Onshore: schematic geological map of the source area with main Italian rivers and Miocene–Quaternary outcropping units. Offshore: digital elevation model for the Adriatic Sea with thickness distribution of sediment deposited in the last 500 year, spanning the Little Ice Age (LIA). The orange dashed line represents the position of the prodelta rollover point (*sensu* Pellegrini *et al.*, 2020). Arrows represent surface circulation (averaged measurements of drifter velocities; Poulain, 2001). Circles represent the location of sediment cores acquired along the western Adriatic shelf. The northern Adriatic sector extends between Po River and Ancona Cape, the Central sector between Ancona Cape and Gargano Promontory, and the southern sector from the Gargano Promontory to the Apulian region.

well-recorded in the Greenland ice cores (Kobashi *et al.*, 2011). During this period, glaciers of the Alps and Apennine mountains expanded (Holzhauser *et al.*, 2005; Giraudi, 2017), associated with changes in vegetation, such as a

marked decrease in tree abundance (Kaplan *et al.*, 2009; Fig. 2). Human-influenced deforestation within watersheds in response to this cold period might have enhanced sediment yields (Oldfield *et al.*, 2003; Giosan *et al.*, 2012; Maselli

& Trincardi, 2013; Renaud *et al.*, 2013; Fig. 2), thus affecting deltaic architecture (Fanget *et al.*, 2014; Pellegrini *et al.*, 2021). This phase of rapid climate change was associated with more recurrent river floods in Europe (Glaser *et al.*, 2010) and a higher frequency of storms along the Mediterranean coasts (Camuffo *et al.*, 2000; Sorrel *et al.*, 2012), which eventually led to enhanced water turbidity in the Adriatic Sea (Fig. 2; Oldfield *et al.*, 2003; Piva *et al.*, 2008).

The Little Ice Age stratigraphic unit and its internal bedsets

The Little Ice Age unit (Fig. 3) comprises strata that extend from the subaerial deltas to their time-correlative fine-grained subaqueous deposits (i.e. compound delta-scale clinoforms, Cattaneo *et al.*, 2003, 2007; Pellegrini *et al.*, 2021). It accumulated over *ca* 350 year and comprises a sediment volume of 60 km³, recording a dramatic increase in sediment supply compared to Mid-Late Holocene deposits (Cattaneo *et al.*, 2003; Amorosi *et al.*, 2016). Basin-scale progradation during the LIA resulted in depocentres up to 10 m thick (Cattaneo *et al.*, 2004; Pellegrini *et al.*, 2021).

Regional chronostratigraphic correlation along the Adriatic mud shelf deposits (Fig. 3) relies on the up-to-date calibration of points of control available from earlier work (summarized in Pellegrini *et al.*, 2021). The bounding surfaces of the LIA stratigraphic unit have been traced and mapped over >600 km based on 30 000 km of CHIRP-sonar profiles, with a typical line spacing of 3 km (Pellegrini *et al.*, 2021; Fig. 3). These seismic horizons, which are locally highlighted by low-angle onlap and downlap terminations and

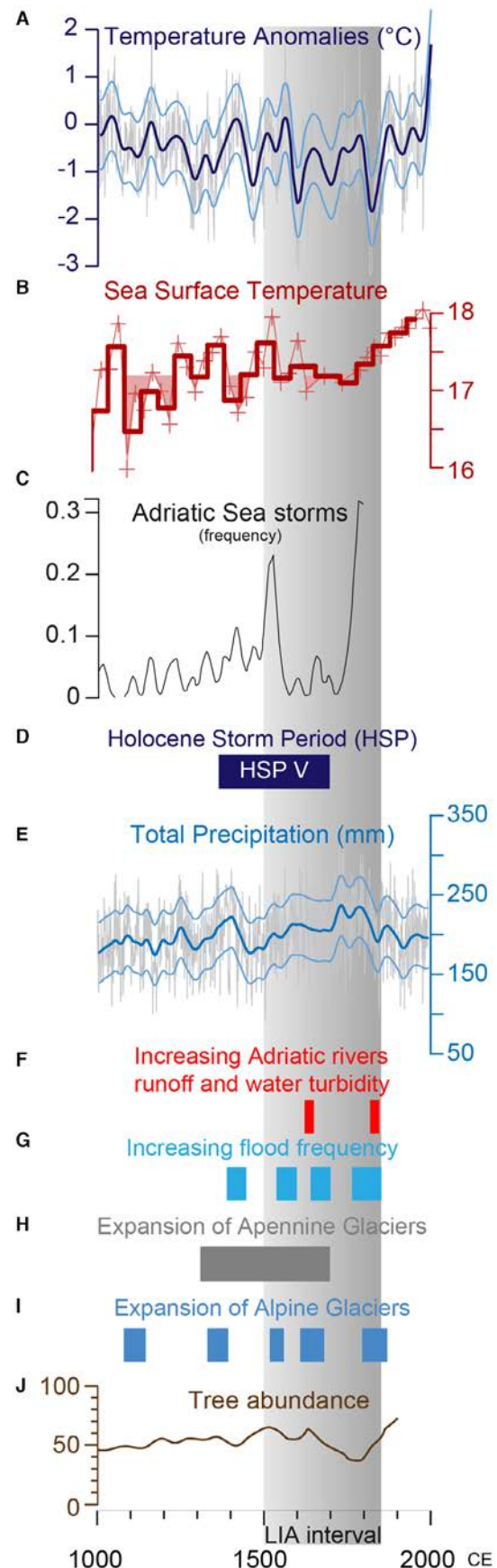


Fig. 2. Multi-proxy reconstructions of climate change in the Northern Hemisphere during the last 1000 years, including the Little Ice Age (LIA, grey bar) showing: (A) European temperature anomalies (Büntgen *et al.*, 2011); (B) sea surface temperature in the Adriatic Sea (Jalali *et al.*, 2018); (C) Adriatic Sea storms (Camuffo *et al.*, 2000); (D) Holocene storm period (HSP, Sorrel *et al.*, 2012); (E) total precipitation (Büntgen *et al.*, 2011); (F) periods of increase in Adriatic Sea water turbidity and river runoff (Oldfield *et al.*, 2003; Piva *et al.*, 2008; Maselli & Trincardi, 2013); (G) increase in river flood frequency (Glaser *et al.*, 2010); (H) expansion of Apennine glaciers (Giraudi, 2017); (I) expansion of Alpine glaciers (Holzhauser *et al.*, 2005); (J) tree abundance (Kaplan *et al.*, 2009).

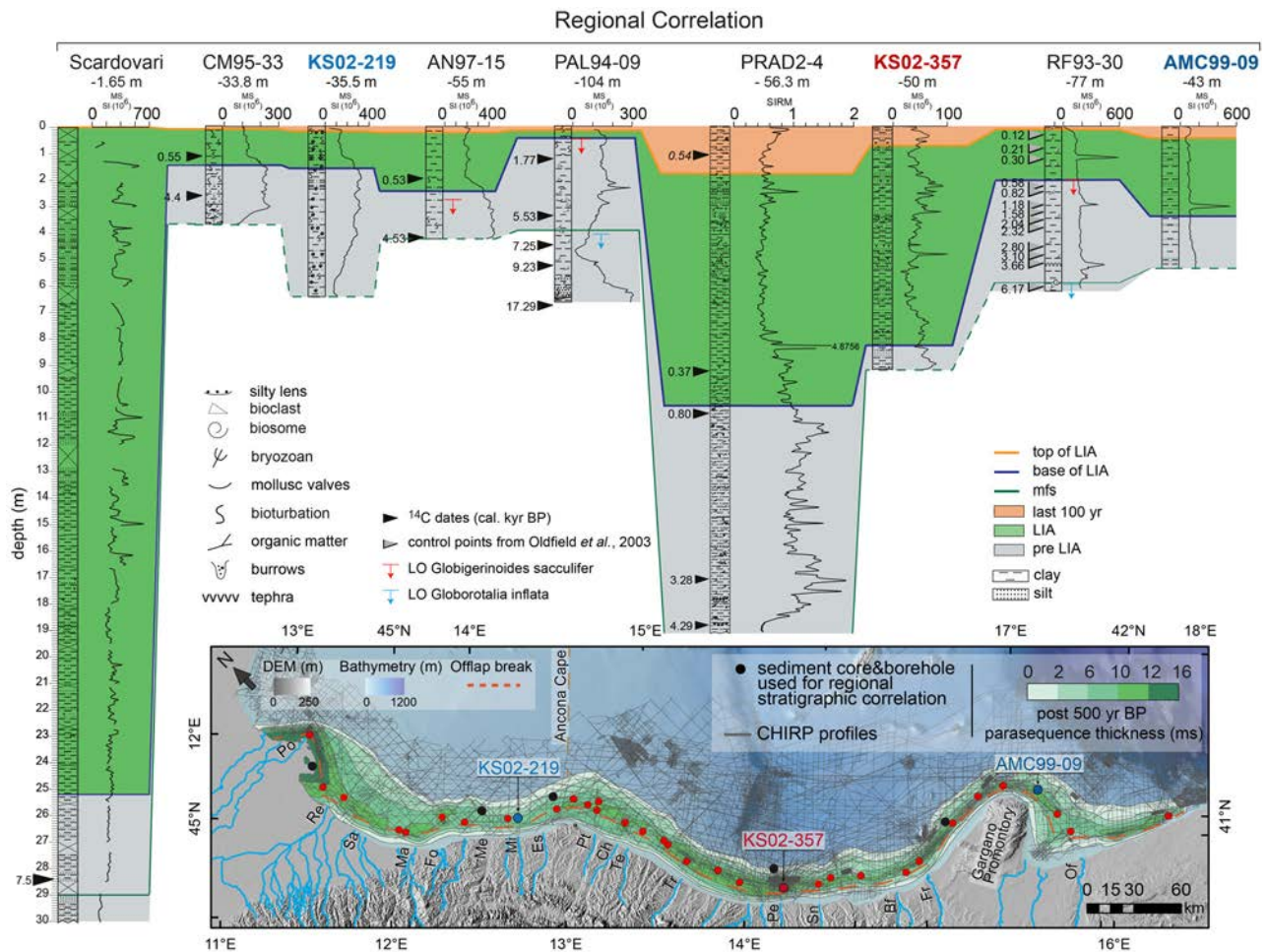


Fig. 3. Top: regional stratigraphic correlation along the Mid-Late-Holocene Adriatic succession, with location of sediment cores and boreholes. Bottom: the stratigraphic database of the Po-Adriatic system. Boreholes include continuous-core descriptions, piston-cores, vibro-cores and gravity-cores. The bathymetry of the Adriatic Sea and thickness of the stratigraphic unit younger than 500 year BP are also reported. Main Italian rivers are represented with abbreviations, as follows: Po River (Po), Reno (Re), Savio (Sa), Marecchia (Ma), Foglia (Fo), Metauro (Me), Misa (Mi), Esino (Es), Potenza (Pt), Chienti (Ch), Tenna (Te), Tronto (Tr), Pescara (Pe), Sangro (Sn), Biferno (Bf), Fortore (Fr), and Ofanto (Of).

bound relatively conformable strata (Pellegrini et al., 2021), can be interpreted as high-frequency (fifth-order) marine flooding surfaces (parasequence boundaries of Van Wagoner, 1995, and Van Wagoner et al., 1988, 1990).

Internally, the LIA unit hosts higher-order bedsets that have been investigated with a vertical resolution of ca 20 cm by Pellegrini et al. (2021). Figure 4 summarizes a tabular compilation and statistical characterization of along-shelf and across-shelf changes in continuity and inclination of the LIA bedsets (Fig. 4). In more detail, the northern Adriatic shelf, between the Po and Esino rivers, hosts high-continuity,

sub-parallel and gently-dipping bedsets (average ca 15 km along-shelf, ca 8 km across-shelf and inclined at 0.29°, respectively). Whereas the central-southern Adriatic shelf, between the Potenza and Biferno rivers, shows the lowest lateral continuity, with more steeply inclined and wavy bedsets (average ca 7 km along-shelf, ca 3 km across-shelf and inclined at 0.7°, respectively). The lowest across-shelf continuities (ca 0.5 km) and higher inclinations (0.9°) are observed in the central Adriatic, offshore the Pescara River, where bedsets show a compensational stacking pattern. The southern Adriatic shelf sector, between the Fortore and Ofanto

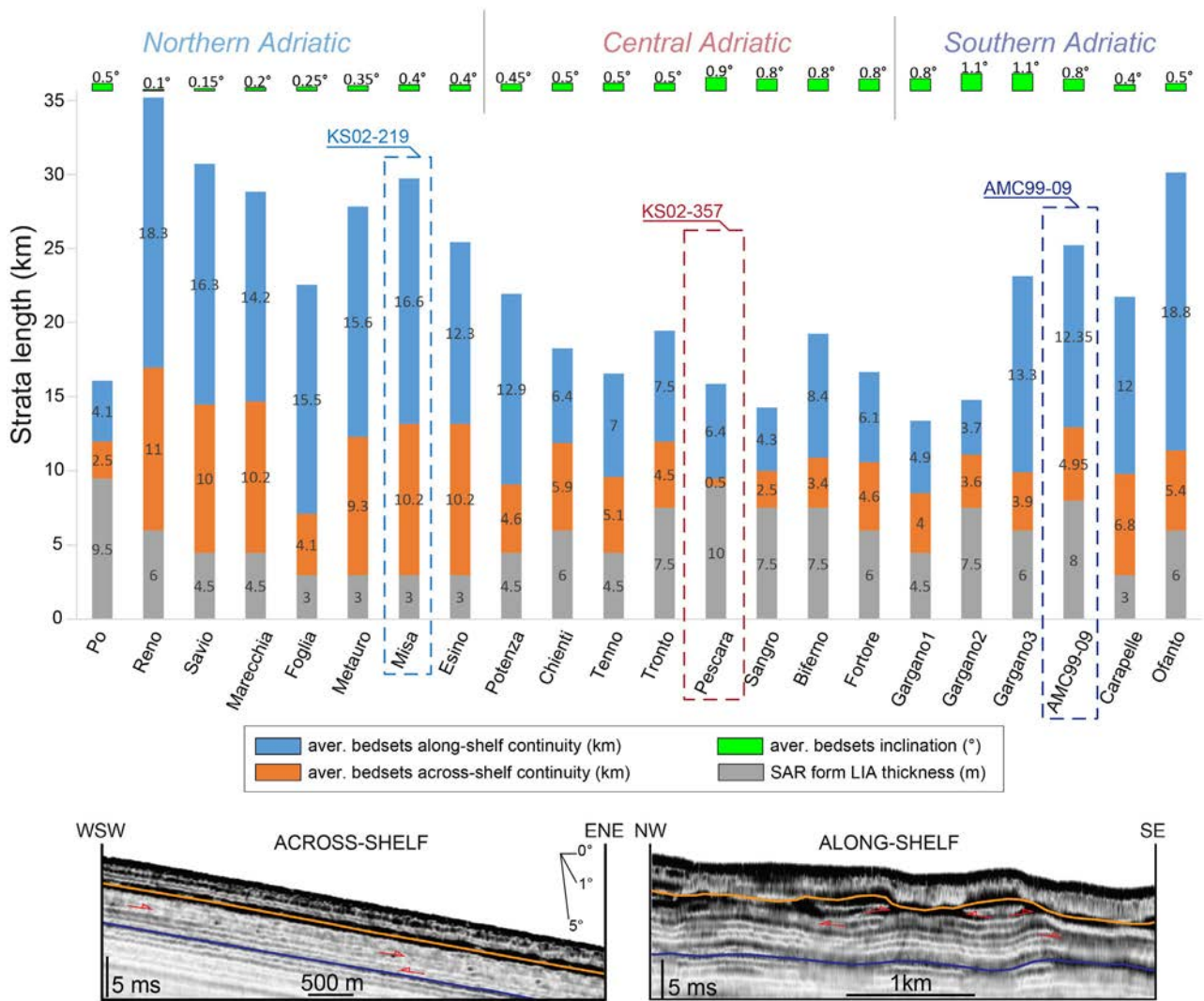


Fig. 4. Top: Bar graph of elemental-bed continuity (length along-shelf and across-shelf) encountered in the coalescing prodeltas of the Little Ice Age (LIA) unit and thickness of LIA deposits along the western Adriatic shelf offshore the main river entry points. Sediment core KS02-357 was retrieved in the Central Adriatic, where bedsets show high inclination (0.9°), the smallest across-shelf continuity (<400 m) and where the LIA unit exhibits the maximum Sediment Accumulation Rate (SAR, 10 m). Bottom: insets show examples of along-shelf and across-shelf CHIRP profiles used for the identification of the LIA bedsets. Modified from Pellegrini *et al.* (2021).

ivers, hosts medium-high continuity, sub-parallel, and steeply inclined bedsets (average *ca* 10 km along-shelf, *ca* 6 km across-shelf and 0.8° inclination, Fig. 4). Following earlier definitions regarding the hierarchy of stratal units (Campbell, 1967), the elemental bedsets consist of stacked beds that are characterized in this work at the sediment core scale. To summarize: in our data base bedsets are visualized on seismic profiles as reflector packages, whereas elemental beds (<50 cm) are defined at the core scale.

Oceanographic setting of the Adriatic basin: where wave and current fields can be measured

The Adriatic Sea is a microtidal environment. Over the western shelf, tidal currents are weak, barely reaching 0.1 m/s, except around capes and promontories (e.g. Cushman-Roisin & Naimie, 2002; Poulain, 2013). The wave climate along the central and southern Italian coast is generally bimodal, with dominant winds from

north-west and south-east (Morucci *et al.*, 2016), the latter along the major axis of the basin. Winds from both the south-east (Sirocco winds) and north-east (Bora winds), can reach gale-force intensity. North-westerly winds are recurrent in summer, but typically milder in this region. According to long-term observations along the western coast of the central and southern Adriatic Sea, the largest significant wave heights are about 5 to 6 m (Morucci *et al.*, 2016).

The dominant circulation of the Adriatic is cyclonic (Fig. 1). Along the western shelf, the flow is south-eastward and includes two distinct components: the Western Adriatic Coastal Current (WACC), which originates as a geostrophic response to river runoff and wind forcing, and the bottom-hugging North Adriatic Dense Water (NADDW; Fig. 1), generated during intense cold outbreaks in the shallow northern Adriatic Sea. While the WACC is a quasi-permanent feature of the circulation in the area, NADDW currents are found only in winters that are cold enough to generate new dense water, thus showing substantial interdecadal variability. The WACC flows along the coast between the 20 m and 50 m isobaths and can easily reach 10 to 20 cm/s (Book *et al.*, 2007; Martin *et al.*, 2009). During windstorms, the WACC can be significantly accelerated, resulting in a vertically integrated current faster than 50 cm/s (Book *et al.*, 2007). The NADDW flows over the shelf at an average speed of 10 to 30 cm/s (Chiggiato *et al.*, 2016); and during windstorms it can accelerate to >40 cm/s (Benetazzo *et al.*, 2014). By the time this current reaches the central/southern sector, it splits into multiple branches that flow off the shelf reaching variable depths downslope (e.g. Sellschopp & Álvarez, 2003; Rice *et al.*, 2013; Chiggiato *et al.*, 2016; Foglini *et al.*, 2016; Marini *et al.*, 2016; Rovere *et al.*, 2019).

Sediment provenance domains, pathways and (disproportional) shelf accumulation

The Po–Adriatic is a multi-sourced foredeep system fed by the Alps in the north, the Apennines in the west and the Dinarides in the east. Each mountain belt is characterized by particular catchment lithologies that can be used to trace distinctive detrital signatures across the whole sediment dispersal system (Amorosi *et al.*, 2022; Fig. 1).

A metamorphic composition is the diagnostic lithic signature of sediment supplied from the Western and Ligurian Alps, where

metamorphic source-rocks are typically associated with granitoid gneisses and metaophiolites (Garzanti *et al.*, 2010; Tentori *et al.*, 2021). In contrast, thick successions of dolostones and limestones are exposed extensively in the Eastern Alps.

The Apennine river catchments consist almost entirely of sedimentary rocks (Fig. 1). Mesozoic carbonate platform to pelagic source rocks (Calcarea Massiccio, Maiolica and Scaglia) are exposed along the upper (western) reaches of Apennine rivers and are especially abundant in the Southern Apennines. Thick Miocene to Pliocene foredeep turbidites (sandstone/marl alternations) of the Marnoso-Areancea Formation and Laga Formation crop out extensively in more eastern positions. The lower parts of Apennine river catchments consist chiefly of Pliocene to Quaternary marine and continental deposits, ranging from sandstones and conglomerates to marls. Finally, the Gargano Promontory belongs to the Triassic–Miocene Apulia platform and consists mainly of carbonate rocks (Fig. 1).

Sediment yield from the Croatian Dinarides is negligible (Cattaneo *et al.*, 2003), reflecting the very small catchment extent, due to location of the mountain divide very close to the coast, and the intensely fractured and karstic nature of the catchments that trap sediment in small basins of the Croatian coastal area (Pellegrini *et al.*, 2017, 2018).

The Po River is one of the largest sources of sediment to the Adriatic Sea (Fig. 1). It originates in the Western Alps and receives sediment from a great number of tributaries that drain the Northern Apennine and Central and Western Alpine chains. Using Quaternary and modern alluvial deposits as compositional endmembers, two key elements (Ni and Cr) and element ratios (Ni/Al₂O₃ and Cr/V) fingerprint Po River sediment sources (Amorosi *et al.*, 2002, 2014, 2022), because high Ni and Cr values are the diagnostic geochemical signature of ultramafic rock successions exposed in the Western Alps and in the north-west Apennines. Conversely, straight and short coastal rivers characterize the Apennine drainage with a geochemical fingerprint of relatively low Ni and Cr contents (Amorosi & Sammartino, 2007).

Although emanating from the mouths of multiple individual rivers, sediment on the shelf is mixed by the oceanographic regime and forms a unique mud shelf deposit whose depocentres are oriented parallel to the coast (Fig. 1). During the last Century, sediment export in the northern sector of the Adriatic shelf (between Po

River and Ancona Cape) exceeded sediment burial, resulting in a net southward sediment bypass (input 16.9 Tg/yr versus sediment accumulation 7.5 Tg/yr); whereas in the central and southern sectors (between Ancona Cape and the Gargano Promontory) sediment burial exceeded the sediment input from local rivers (input 7.8 Tg/yr versus 13.9 Tg/yr sediment accumulation; Frignani *et al.*, 2005).

The lithological composition of the Po–Adriatic catchments and the oceanographic setting play a fundamental role in controlling the distribution of trace metals within Adriatic shelf sediments. Despite along-shore mixing and increasing dilution with sediment sourced from Apennine river catchments, Cr-rich and Ni-rich detritus generated in mafic and ultramafic complexes of the Western Alps, and conveyed through the Po River into the Adriatic Sea via the Western Adriatic Current, records a basin-wide geochemical signal that can be traced downdrift as far as 1000 km within Adriatic shelf muds, from the Alpine zone of sediment production to the area of final deposition, offshore Apulia (Amorosi *et al.*, 2022).

Many of the rivers contain only first-order and second-order branches, 50 to 150 km in length. These small catchments (500–3300 km² area) are rugged (1000–3000 m elevation) and give rise to rivers with high sediment yields. Presently, the sediment load of Apennine rivers passes through numerous small reservoirs with sediment trapping efficiencies in the range of 20 to 50% (Mancinelli, 2000). Among the Apennine rivers, the Pescara River is *ca* 150 km long, with a drainage area of 3300 km² and a relief of 2700 m.

APPROACH, DATA AND METHODS

Depositional processes that formed the LIA beds were reconstructed by combining analysis of sedimentary structures and their vertical stacking, grain-size grading patterns, bioturbation intensity, meiofauna (benthic foraminifera and ostracods), lignin, and trace metal contents (Table 1). Because the modern Adriatic physiographic setting is similar to the LIA palaeogeography, an oceanographic model of the wave field and current pathways was implemented to validate the reconstructed depositional processes with the well-known modern oceanographic regime.

Facies characteristics were examined in detail by combining complementary proxies and tools with lamina to bed-scale observations to explore sediment source, type of transport, and

Table 1. Facies key and Meiofauna Ecological Categories for the sedimentological sections presented in this study.

Lamina geometry — planar, parallel — curved, nonparallel — wavy, parallel — wavy, nonparallel	Facies associations Along-shelf current deposit Hy Hyperpycnite deposit St Storm deposit
Sedimentary structures — wave ripple — current ripple — ripple cross-laminations	Grain size clay silt μ mm
Fossils and biogenic structures — bioclasts & bivalves — escape structure — burrow — wood fragment	Meiofauna Ecological Categories (ECs) Benthic Foraminifera — opportunistic taxa — indifferent+ sensitive taxa — not assigned taxa Ostracoda — opportunistic mud loving taxa — sandy pebble loving taxa — sand loving taxa — not assigned taxa * <100 valves, but more than 10 ** <10 valves

depositional conditions. A bed is considered herein as a relatively conformable succession of genetically related laminae or laminasets bounded at base and top by bedding surfaces of erosion (rare in the Adriatic sediment cores), non-deposition, or correlative conformity (Campbell, 1967). Sedimentary structures, at lamina and bed scale, and changes in sediment provenance were investigated along-strike within the LIA prodelta slope, with a particular emphasis on where the terrestrial biomarkers (i.e. lignin phenols) were deposited, and on the main processes that drove sediment delivery, transport and deposition.

Sedimentological analysis

Sedimentological analysis was conducted on selected piston sediment cores (recovery >90%) representative in terms of sedimentary structures of the northern, central, and southern LIA unit. The cores were collected in coalescing prodeltas (KS02-219, KS02-357 and AMC99-09 cores, 6.4 m, 9.16 m, and 4.0 m long, respectively) at 35.5 m, 50.0 m and 43.0 m water depths (Fig. 1). Sediment-core description, coupled with high-resolution digital X-ray images, was carried out to characterize grain size, bedding thickness, porosity and subtle sedimentary structures, as well as bioturbation intensity (Table 1; Bioturbation Index, BI, by Taylor & Goldring, 1993). In the present study, beds measured in the prodelta slope facies range in thickness from 1 to 50 cm. A total of *ca* 200 beds were described along a total thickness of 13 m of the LIA in cores KS02-219, KS02-357, and AMC99-09 (Figs 5, 6, and 7). A subset of samples, characterized by evident changes in texture, was selected for Scanning Electron

KS02-219 (Northern prodelta slope, 35.5 m w.d.)

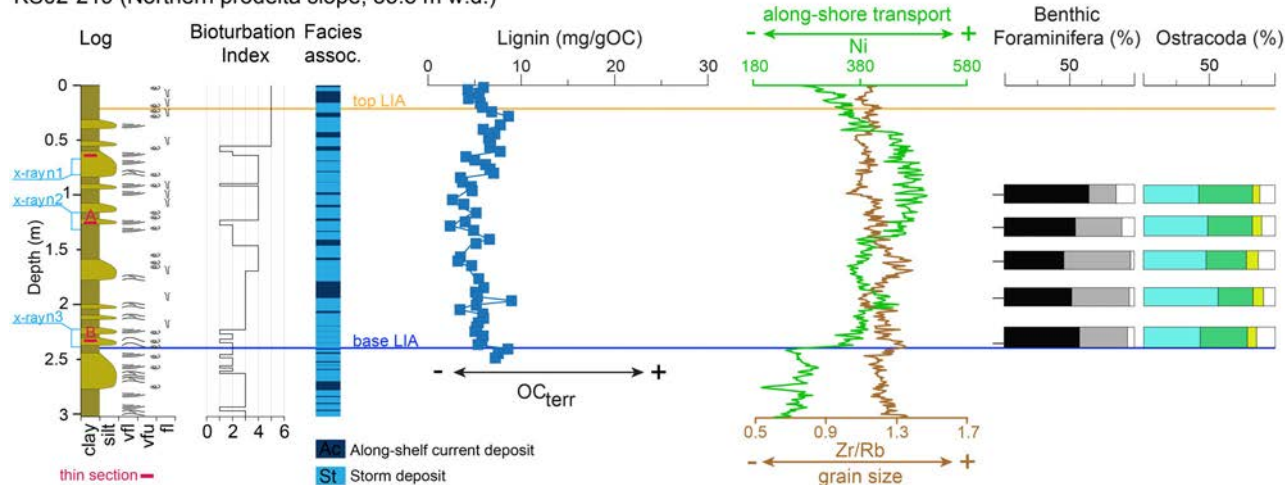


Fig. 5. Sediment core log from the Northern Adriatic prodelta slope integrated with the Bioturbation Index (BI) log, sedimentary facies, lignin content, Ni and Zr/Rb abundances, and meiofauna relative abundances in terms of ecological categories. The facies points towards a storm-dominated system. Blue square brackets represent X-ray insets reported in Fig. 8. Red rectangles indicate thin section samples; scanning electron microscopy (SEM) images of thin section 'A' and 'B' are reported in Fig. 9.

Microscope (SEM) analyses to detect diagnostic sedimentary structures (millimetre to centimetre-scale) and sedimentary textures (millimetre to micron-scale features, particle organization). Turning sediment from a near liquid state (60 or more volume % water) into a solid was achieved by replacing pore waters (via stepwise diffusion) with Spurr resin and then hardening the resin through heat treatment (Schimmelmann *et al.*, 2015). The resulting solid was sectioned for examination of sedimentary structures by petrographic microscope and was argon ion milled for the study of sediment fabrics by electron microscopy (Schieber, 2016). Textural and compositional variability of the LIA beds were characterized providing complementary information on the depositional environment, in terms of mud transport (i.e. low/high energy environment), accumulation and compaction (i.e. porosity), provenance (at lithics scale), and diagenesis (i.e. diagenetic products or authigenic minerals, such as pyrite, glauconite, and cements).

Geochemical analyses

The interpretation of sedimentary structures was then combined with geochemical analyses on both organic and inorganic proxies to understand nature and provenance of the sediment, respectively. Lignin data for KS-02 219 and KS02-357 were taken from the literature (Pellegrini *et al.*,

2021), whereas new data were generated for AMC99-09 following the same analytical method (see also Gordon & Goñi, 2003). The content of terrestrial organic carbon (OC) in the LIA beds obtained through terrestrial biomarkers is very helpful, especially in the case of beds whose primary sedimentary structures have been destroyed by bioturbation.

Geochemical analysis by X-ray fluorescence (XRF) core scanning has become a well-accepted and widely used analytical method to investigate the elemental composition of marine and terrestrial sediments (Rothwell & Rack, 2006; Weltje & Tjallingii, 2008; Thöle *et al.*, 2019). Core surfaces were cleaned carefully and then scanned at the Institute of Marine Science (CNR-ISMAR, Bologna) using an AVAATECH μ XRF core scanner (AVAATECH, Dodewaard, The Netherlands). Measurements were carried out using a rhodium type anode set at 10, 30 and 50 kV with a resolution of 1 cm. The XRF spectral data were then converted to a record of net element intensities expressed as counts per second (cps). For the chemostratigraphic interpretation of geochemical data, vertical trends in element abundance were used rather than absolute values.

Meiofauna analysis

A quantitative analysis of the meiofauna was performed on 12 sub-samples (1 cm thick) to support

the reconstruction of bottom conditions, especially in terms of organic enrichment, turbidity, oxygen level and vegetation cover. The selection of samples was aimed at improving the facies characterization in each of the three distinct sectors of the LIA prodelta slope (KS02-219, KS02-357 and AMC99-09 cores). Approximately 30 g of dry sediment were treated for each sample, following the methodology reported in Rossi & Vaiani (2008) that includes soaking overnight in 10% H₂O₂, water-screening with a 63 µm sieve and drying again for >8 h. The size fraction >125 µm was split into small portions and at least 100 well-preserved tests of benthic foraminifera and 100 ostracod valves (with carapaces considered as two valves) were counted (Table S1; Fig. S1). Any other shell material was noted as well. Both adult and juvenile ostracod valves that allowed identification at species level were counted. The relevant literature for taxonomic identification and palaeoecological interpretation includes several works dealing with the modern and late Quaternary shallow-marine meiofauna of the Mediterranean Sea (e.g. Bonaduce *et al.*, 1975; Breman, 1975; Jorissen, 1988; Sgarrella & Moncharmont Zei, 1993; Fiorini & Vaiani, 2001; Milker & Schmiedl, 2012; Jorissen *et al.*, 2018; Aiello *et al.*, 2020). On the Adriatic shelf, besides water depth, organic-matter concentration and grain size are the main environmental drivers for benthic foraminifera and ostracods, respectively (Barbieri *et al.*, 2019, and references therein). Thus, the meiofauna dataset was optimized using ecological categories (Table S2). For benthic foraminifera, the Mediterranean categories defined by Jorissen *et al.* (2018) based on organic-matter gradients (i.e. sensitive – indifferent – third-order opportunistic – second-order opportunistic – first-order opportunistic) were adopted, focusing on opportunistic *versus* indifferent+sensitive taxa. For ostracods, based on modern distribution patterns across the Adriatic Sea (Bonaduce *et al.*, 1975; Breman, 1975; Barbieri *et al.*, 2019), three main categories were identified: opportunistic taxa preferring: (i) muddy; (ii) sandy mud; and (iii) sandy substrates. Taxa without specific ecological requirements were gathered into the ‘not assigned’ category (<10–15% for both meiofauna groups within the studied cores).

Oceanographic modelling – ocean surface wave data

A multi-decadal time series of two datasets was used to define (modern) wave climate. For the

analysis, model data and wave buoy records were considered, extending across the periods 1993 to 2021 and 1989 to 2008, respectively. The model dataset comes from the Copernicus Marine Environment Monitoring Service (CMEMS), in particular from the multi-year Mediterranean Sea Waves Reanalysis (Korres *et al.*, 2021) product, with a wave period resolution of 0.5 s and a grid of 0.042° × 0.042°, simulating the period 1993 to 2021. Wave records were obtained from measurements of the Italian National Wave Network supplied by the wave buoys of Ortona (<https://www.mareografico.it>) and Monopoli (<http://dati.isprambiente.it/dataset/ron-rete-ondametrica-nazionale/>).

The Wave Base (WB), defined as one-half of the wavelength, marks a shelf sector impacted by the wave field. Modelling of the WB provides further support in the reconstruction of depositional processes from sedimentary analysis. In addition to significant wave height and peak period, readily available in both datasets, the wavelength to compute the WB was derived from the peak period following linear wave theory, in two steps: first, the 95th significant wave height percentiles of the dataset were used to select intense storms able to influence coastal transport with a reasonable annual frequency; then, the median peak period of the selected waves was used to compute the WB.

RESULTS

Three main types of sedimentary facies were distinguished; storm-dominated, river-dominated and drift-dominated facies within the LIA climothems of the Adriatic shelf.

Sedimentary facies of the Little Ice Age stratigraphic unit

Storm-dominated facies

Description. A total of 19, 18, and 6 storm-related beds were counted in sediment cores KS02-219, KS02-357, and AMC99-09, respectively (Figs 5, 6, and 7). The storm-dominated sedimentary facies consists of clay–very fine silt in structureless beds >5 cm thick enriched in shells (mostly *Turritella*) interspersed within >5 cm beds with curved laminae, locally top-truncated and associated with bioclasts and with hummocky cross-stratification (Fig. 8, n1, n2, and n3); in addition, wave ripples are recorded by top-truncated laminae and hints of swaley

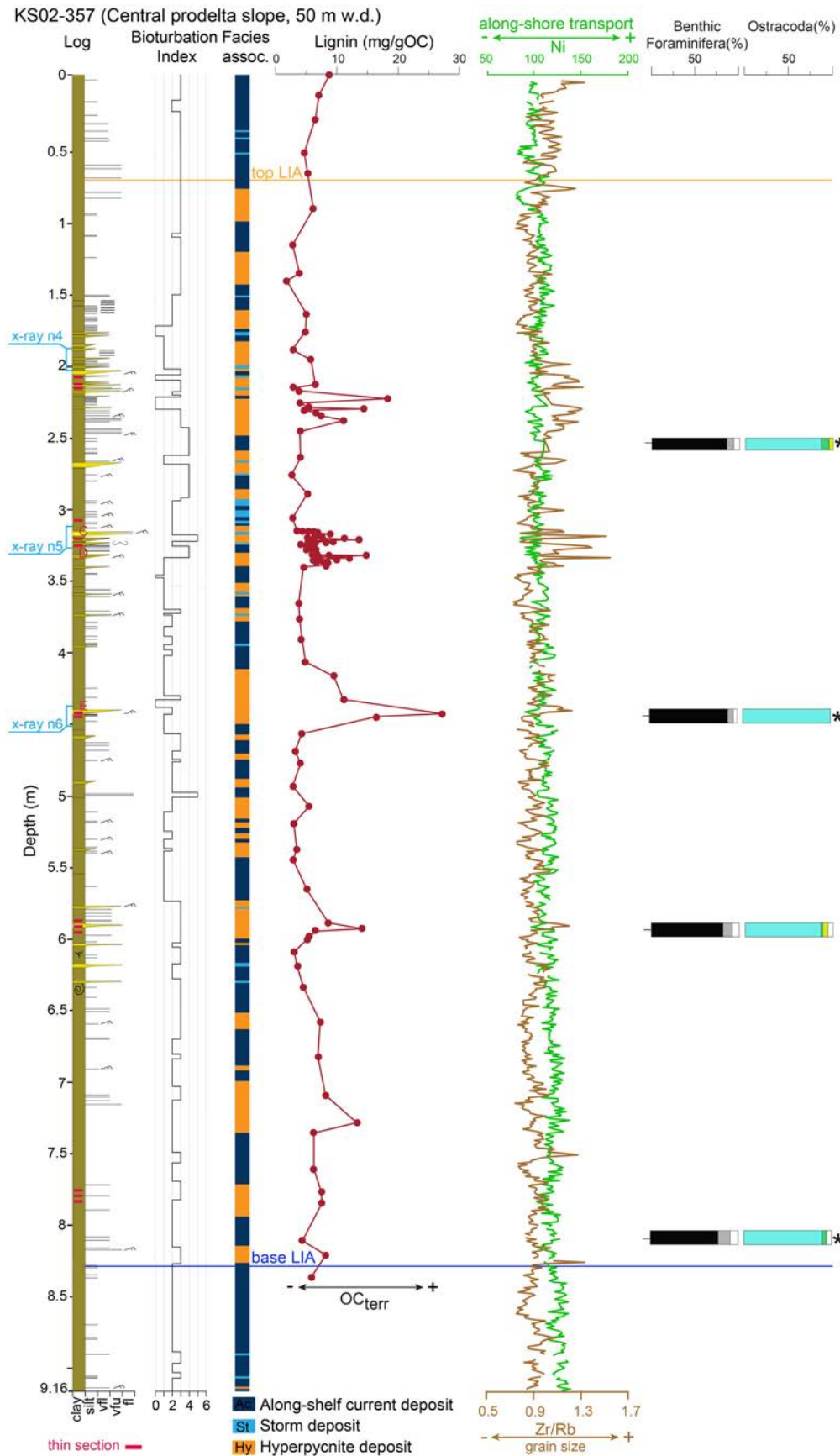


Fig. 6. Sediment core log from the Central Adriatic prodelta slope integrated with the Bioturbation Index (BI) log, facies, lignin content, Ni and Zr/Rb abundances, and relative abundances of meiofauna in terms of ecological categories (*less than 100 valves, but more than 10); note that the lignin content is the highest encountered along the Little Ice Age (LIA) unit. The facies points towards a river-dominated system. Blue square brackets represent X-ray insets reported in Fig. 8. Red rectangles indicate scanning electron microscopy (SEM) samples; SEM images of samples 'C', 'D', and 'E' are reported in Fig. 10. For graphical reasons, the vertical scale is approximately double compared to the vertical scale of cores KS02-219 and AMC99-09.

cross-lamination (Fig. 8, n3). In storm-related beds, the Bioturbation Index (BI) varies from 4 to 5 and rarely attains a value of 2 (Figs 5, 6, and 7). The lignin content is relatively constant throughout the facies, between 2.0 and 7.0 mg/g OC, and shows low-amplitude oscillations within each bed (Figs 5 and 7). These values are accompanied by relatively high (>300) Ni counts and Zr/Rb (*ca* 1) values (Figs 5 and 7). Thin section analysis shows poorly sorted mudstone matrix (Fig. 9, A1 and B1), including fossil coccolith debris (Fig. 9, B2). Small burrows are well-preserved (Fig. 9, A1). Mafic grains, such as mafic inclusions (possibly clinopyroxene), in K-feldspar and altered biotite (Fig. 9, A2) are common. Detrital calcite, dolomite, and quartz

grains, as well as mica and altered biotite flakes are common (Fig. 9, B3, and B4).

The meiofauna is highly diversified, showing the co-occurrence of infralittoral to circalittoral species with different degrees of tolerance to organic content and substrate grain-size. The foraminiferal fauna is typified by slightly higher amounts of opportunistic taxa (*ca* 45–65%) compared to sensitive+indifferent (*ca* 20–50%) taxa. The former are mostly represented by species favoured by the first stages of organic enrichment (for example, *Aubignyna perlucida*, *Bulimina* and *Textularia* species), whereas the latter mainly include *Criboelphidium decipiens* and epiphytic taxa. The ostracod fauna shows an almost equal number of taxa preferring organic-

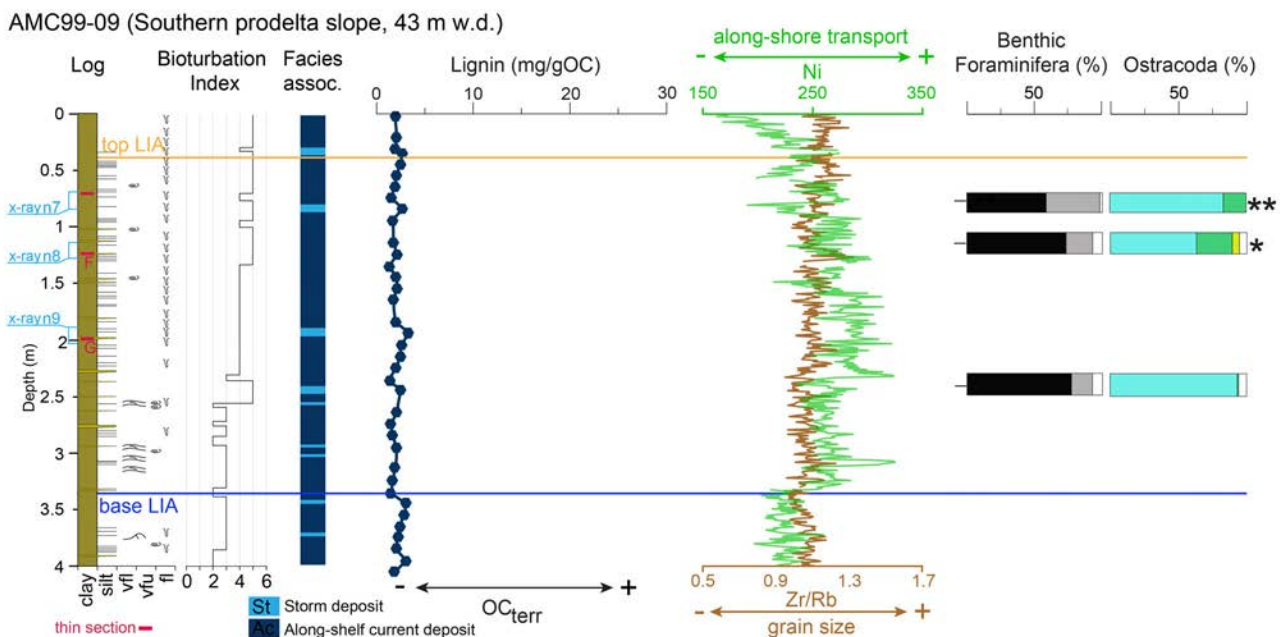


Fig. 7. Sediment core log from the Southern Adriatic prodelta slope integrated with the Bioturbation Index (BI) log, facies, lignin content, Ni and Zr/Rb abundances, and relative abundances of meiofauna in terms of ecological categories (*less than 100 valves, but more than 10; **less than 10 valves); note that the lignin content is the lowest encountered along the Little Ice Age (LIA) unit. The facies points towards a drift-dominated system. Blue square brackets represent X-ray insets reported in Fig. 8. Red rectangles indicate scanning electron microscopy (SEM) samples; SEM images of samples 'F' and 'G' are reported in Fig. 11.

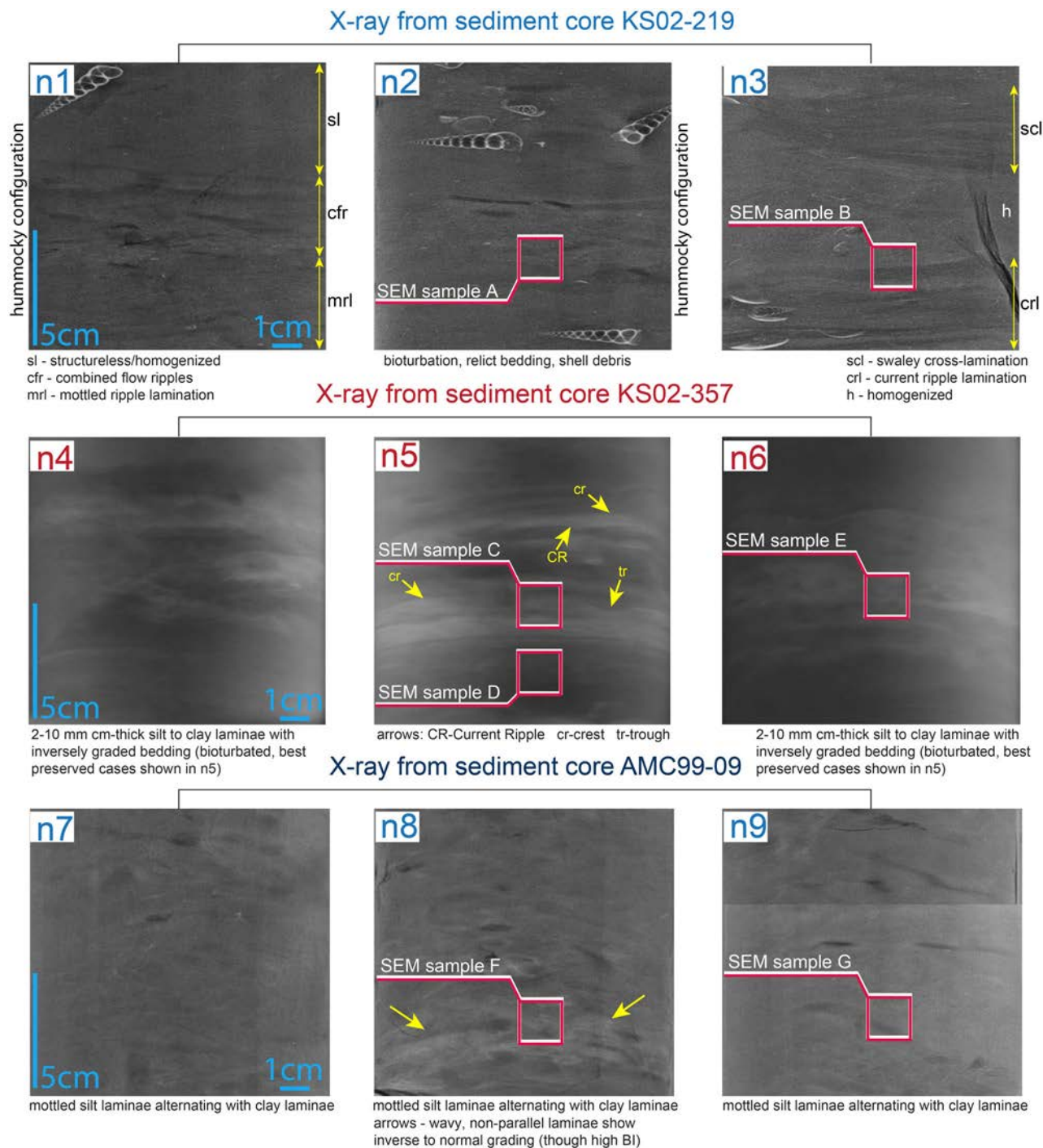


Fig. 8. X-rays (20×8 cm) of key portions of sediment cores. Top: insets from KS02-219 with clay-very fine silt in structureless beds enriched in shells and beds with curved laminae, locally top-truncated and associated with current ripples, bioclasts and hummocky configuration. Locally, swaley cross-lamination is preserved. Centre: insets from KS02-357 with stacked beds constituted by discrete 2 mm to 1 cm thick silt to clay laminae with graded bedding. Laminae overlie sharp surfaces, forming lamina-sets of current ripples with sharp, narrow, relatively straight and climbing crests between broadly rounded troughs. Bottom: insets from AMC99-09 showing mottled silt laminae alternating with clay laminae. Beds are strongly bioturbated, with primary structures difficult to discern, although locally, wavy, non-parallel laminae show inverse to normal grading. Red squares in X-ray images highlight areas of the scanning electron microscopy (SEM) samples reported in Figs 9, 10 and 11.

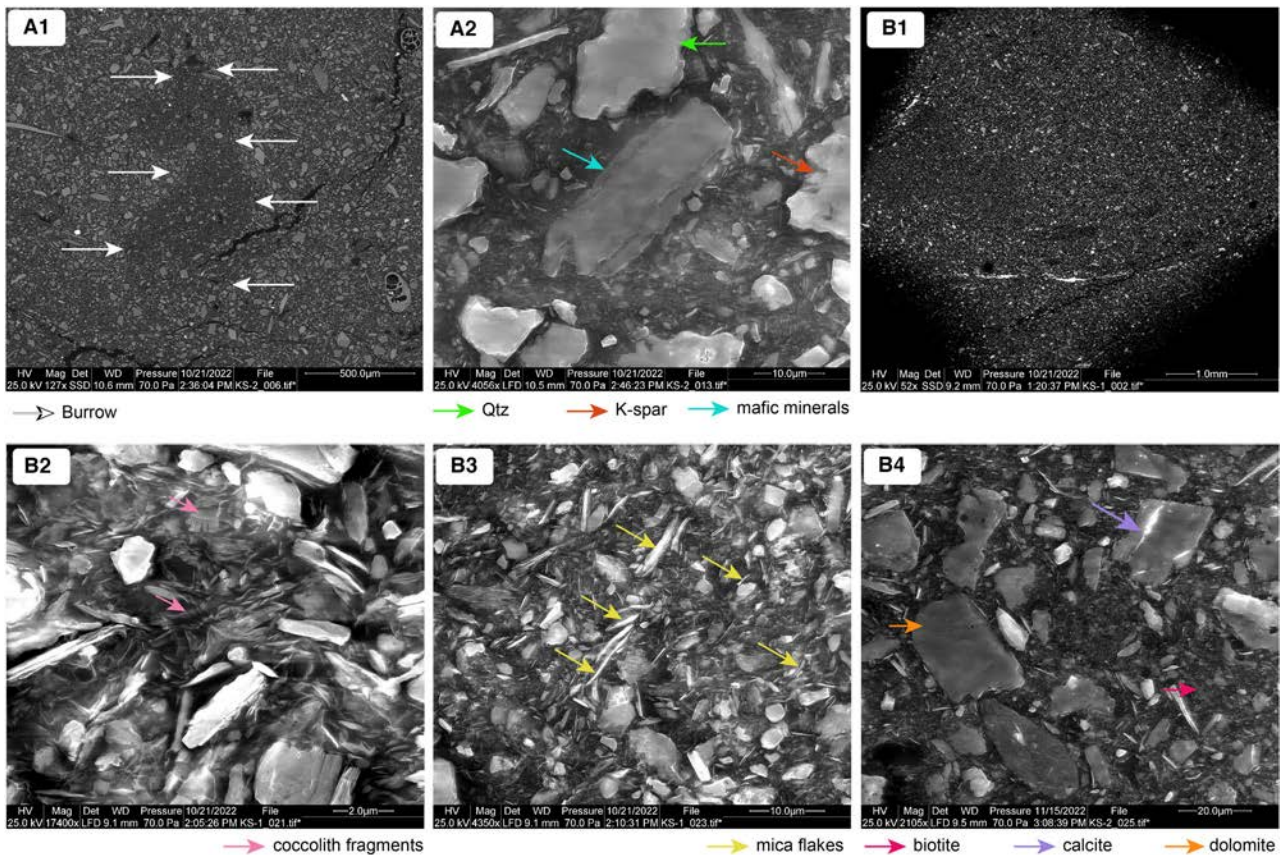


Fig. 9. Scanning electron microscopy (SEM) images from ion milled sections of sediment core KS02-219 (see Fig. 8) showing: (A1) burrow; (A2) quartz (green arrow), K-feldspar (brown arrows) and mafic minerals (blue arrows), possible clinopyroxene and flakes of altered biotite; (B1) poorly sorted, coarse-grained fabric with small burrows (darker spots); (B2) mud matrix with coccolith debris (pink arrows); (B3) mica flakes (yellow arrows); (B4) detrital calcite (violet arrows), dolomite grains (orange arrows) and altered biotite (red arrow).

enriched muddy bottoms (*ca* 40–55%; mainly *Cytheridea neapolitana*) and taxa preferring sandy–pelitic environments (*ca* 25–40%; mainly *Hiltermannicythere turbida*; Figs 5 and 7).

Interpretation. Diagnostic structures, such as hummocky cross-stratification and upward-fining truncated laminae suggest deposition under combined-flow erosion and traction transport followed by suspended load to suspension settling from waning currents, as documented elsewhere for storm-dominated deposits (Nummedal & Swift, 1987; Arnott & Southard, 1990; Lazar *et al.*, 2015b; Grundvåg *et al.*, 2021; Schwarz *et al.*, 2021). The relative increase in Ni content suggests a sediment supply mainly from the Po River (Amorosi *et al.*, 2022). Coccolith debris and detrital carbonate grains suggest provenance from limestones and marls of the Umbria-Marche

Succession (Fiorentino, 1994) cropping out in the Misa and Metauro river catchments (Fig. 1). Concurrently, low lignin content and the variety and composition of the meiofauna (i.e. co-existence of opportunistic, sensitive and epiphytic taxa) are indicative of a marine setting affected by scarce OM fluxes, redistributed over the seafloor by currents, and characterized by relatively low turbidity and muddy bottoms with vegetation patches (Frezza & Di Bella, 2015; Rossi *et al.*, 2021).

River-dominated, prodelta slope facies

Description. Forty-one river-related beds were counted in sediment core KS02-357, whereas this sedimentary facies was not encountered in sediment cores KS02-219 and AMC99-09 (Figs 5, 6 and 7). The river-dominated sedimentary facies is represented by 2 mm to 1 cm thick very fine sand/silt to clay laminae showing inverse to

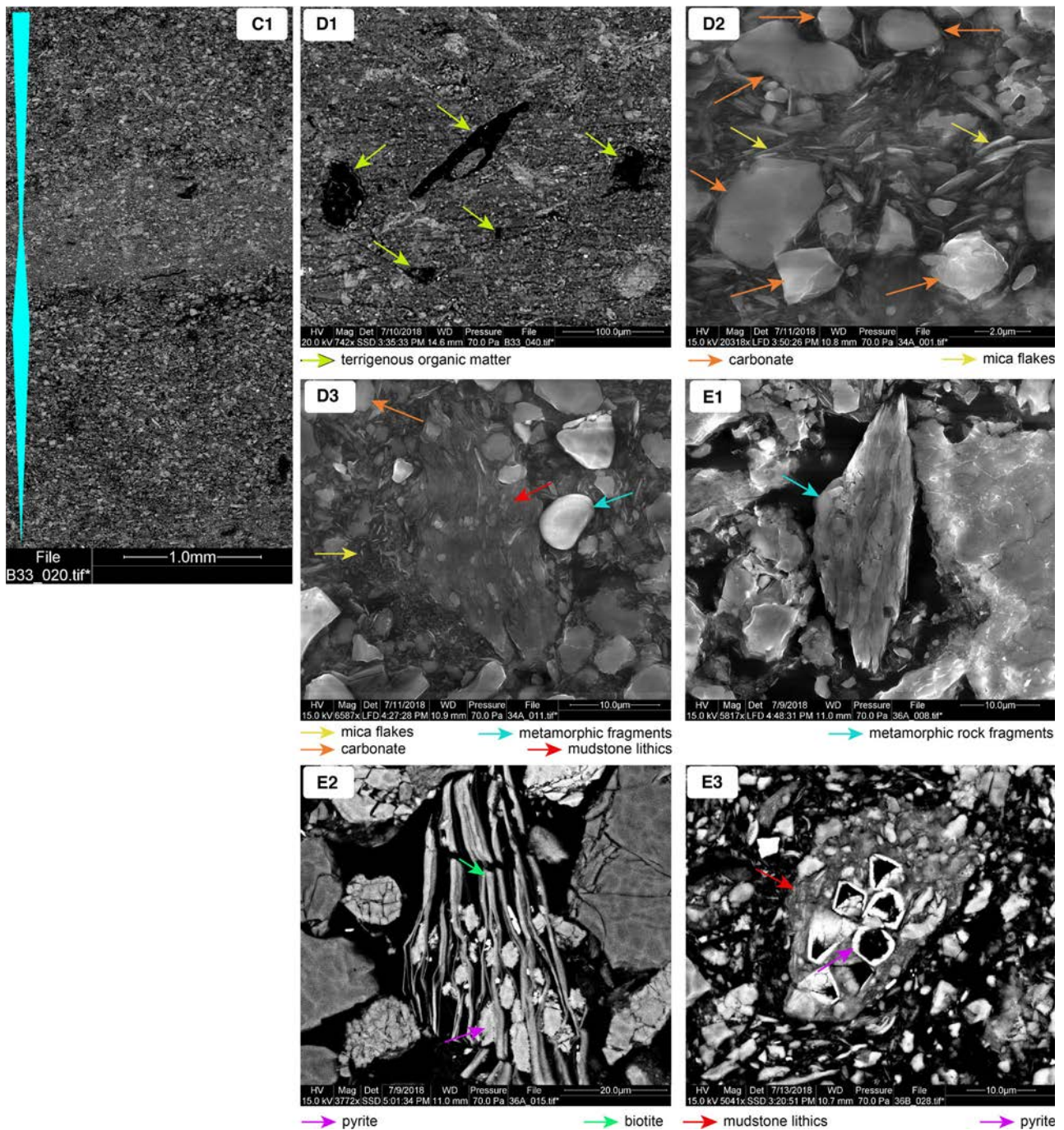


Fig. 10. Scanning electron microscopy (SEM) images from ion milled SEM mounts prepared for core KS02-357 (see Fig. 8) showing: (C1) alternating clay-rich and silt-rich laminae that show inverse to normal grading consistent with hyperpycnal deposits; (D1) well-preserved plant fragments up to 100 microns in size; (D2) carbonate fragments (brown arrows), clay and mica flakes (green arrows), (D3) mudstone lithic (red arrows), mica flakes (yellow arrows) and carbonate fragments (orange arrows); (E1) metamorphic (schist or slate) rock fragment of silt size (blue arrow); (E2) pyrite between sheets of a degraded biotite grain, suggesting diagenetic pyrite formation in sulfidic pore waters; (E3) mudstone lithic (red arrow) with Fe-oxide pseudomorphed pyrite (purple arrows) that probably were oxidized during outcrop weathering and pseudomorphed by a (bright) iron oxide rim.

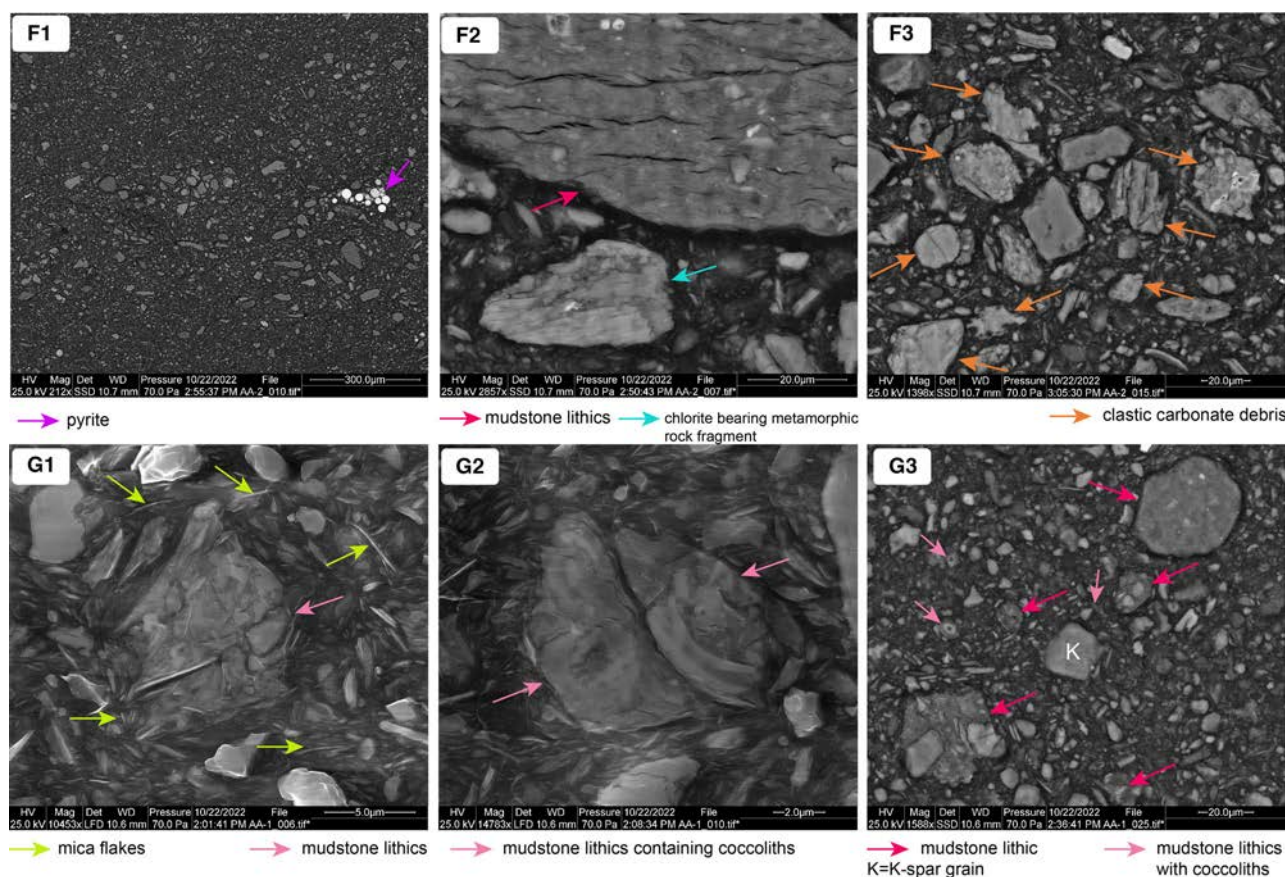


Fig. 11. Scanning electron microscopy (SEM) images of ion milled samples from sediment core AMC99-09 (see Fig. 8) showing: (F1) bioturbated sediment texture with abundant mudstone lithics, detrital carbonate debris; framboidal pyrite (purple arrow) is localized suggesting diagenesis non-sulfidic pore waters; (F2) large mudstone lithic (red arrows) and a chlorite-bearing metamorphic rock fragment (blue arrows); (F3) detrital carbonate particles (orange arrows); (G1) mica flakes (green arrows) and mudstone lithics (pink arrows); (G2) mudstone lithics containing coccoliths (pink arrows); (G3) mudstone matrix with mudstone lithics and coccoliths.

normal grading (Figs 5, 6 and 7). Laminae overlie sharply defined surfaces, forming lamina-sets of current ripples with sharp, narrow, relatively straight and climbing crests between broadly rounded troughs (Fig. 8, n4, n5 and n6). Internally, laminae are convex up and lap down on basal surfaces (Fig. 8, n4, n5 and n6). The BI varies from 1 to 2 and rarely attains 3, the highest values being associated with clay-dominated beds (Fig. 6). Well-defined laminated intervals showing inverse to normal grading correspond to lignin-rich sediments (up to 27.2 mg/g OC), with distinctly low Ni values and high Zr/Rb ratios (Fig. 6).

At the SEM level, alternating clay-rich and silt-rich laminae show inverse to normal grading and contain detrital carbonate, clay and mica flakes (Fig. 10, C1–D3); plant fragments up to 100 microns

in size are well-preserved (Fig. 10, D1). Mudstone and metamorphic rock fragments (lithics) are also present (Fig. 10, D2–E3). Metamorphic rock fragments and mica flakes, variably altered and deformed, can reach the coarse silt size (Fig. 10, D3 and E1). Pyrite is present between sheets of degraded biotite grains, suggesting diagenesis in sulfidic pore water (Fig. 10, E2). Mudstone lithics can contain pyrite grains that likely were oxidized during outcrop weathering and pseudomorphed by a (bright) iron oxide rim (Fig. 10, E3).

The meiofauna is characterized by the strong dominance of taxa preferring ample food availability (i.e. organic matter) at water depths >20 m. Opportunistic taxa compose *ca* 80 to 90% of the foraminiferal assemblage and are mainly represented by *Valvulineria bradyana* with the secondary occurrence of *Bulimina* species. By contrast,

sensitive and epiphytic taxa are almost absent. Three out of four samples contained less than 100 ostracod valves (minimum value is 22 in the uppermost sample; Table S1) and showed the dominance (>85%) of mud-loving taxa able to tolerate high organic contents. In particular, *C. neapolitana* is the dominant species by far (ca 45–50%), with *Leptocythere ramosa* and *Palmococoncha turbida* as accompanying species (Figs 5, 6 and 7).

Interpretation. The lignin-rich, laminated intervals, showing inverse to normal grading at both bed and lamina scales are attributed to hyperpycnites (e.g. Mulder *et al.*, 2003; Mutti *et al.*, 2003; Zavala *et al.*, 2011; Li *et al.*, 2015) and thought to reflect the record of river flood pulses in the prodelta slope (Pellegrini *et al.*, 2021). Peaks in the Zr/Rb ratio denote a markedly coarser grain size of these layers (Dypvik & Harris, 2001; Chen *et al.*, 2009). A river-dominated depositional system, supplied exclusively by Apennine rivers without influence from the Po, is suggested by comparatively low Ni counts and by an abundance of carbonate rock fragments (Amorosi *et al.*, 2022). The local presence of metamorphic rock fragments likely reflects sediment contribution from the Aterno-Pescara catchment, where 50% of fine-grained lithics in the turbiditic Laga Formation are of metamorphic origin (Chiocchini & Cipriani, 1992). The composition of the meiofauna points to a marine setting subject to substantial influx of OM and fine particles (Frezza & Carboni, 2009; Frezza & Di Bella, 2015; Goineau *et al.*, 2015; Rossi *et al.*, 2021). Under these eutrophic conditions, decreases in oxygen levels can occur occasionally, as suggested by the pervasive presence of species that can tolerate oxygen deficiency, such as *V. bradyana*, *Bulimina* spp. and *Palmococoncha turbida* (Van der Zwaan & Jorissen, 1991; Frezza & Di Bella, 2015). The overall paucity of ostracod valves likely points to high turbidity and high accumulation rates, physical characteristics that are typical of muddy shelf deposits (Bhattacharya *et al.*, 2020).

Drift-dominated, prodelta slope facies

Description. A total of 12, 36, and 28 drift-related beds were counted in sediment cores KS02-219, KS02-357 and AMC99-09, respectively (Figs 5, 6, and 7). The drift-dominated sedimentary facies shows mottled silt laminae alternating with clay laminae (Fig. 8, n7, n8 and n9). In places, wavy, non-parallel laminae showing

inverse to normal grading are preserved (Fig. 8, n7, n8 and n9). The BI varies from 4 to 5 and rarely drops to 3 (Figs 5, 6 and 7). The lignin content is low throughout the facies, and generally lower than 5.0 mg/g OC (Figs 5, 6, and 7). The nickel content is high throughout the LIA stratigraphic unit, whereas Zr/Rb ratios are relatively low (Figs 5, 6, and 7).

At the SEM level, the sediment texture is homogenized due to bioturbation. The sediment contains abundant mudstone lithics (some containing coccoliths), detrital carbonate debris and muscovite flakes (Fig. 11, F1–F3, G1–G3). Locally, mudstone lithics show concentrations that form wavy laminae (Fig. 11, F1). Chlorite-bearing metamorphic rock fragments are also present (Fig. 11, F2). Framboidal pyrite is localized (Fig. 11, F1), suggesting formation in anoxic and non-sulfidic pore waters (Berner, 1981; Brett & Allison, 1998; Schieber, 2002).

Taxa preferring organic-enriched substrates typify the meiofauna, which is quite scarce, especially for the ostracod fraction (Table S1). As for benthic foraminifera, opportunistic taxa reach ca 60 to 75% and are mainly represented by *V. bradyana*, *Bulimina* spp. and *Melonis affinis*. Indifferent taxa, such as *C. decipiens* (up to 20%) are dominant over sensitive. Epiphytic taxa are scarce (<5%). The ostracod fauna contains abundant opportunistic mud-loving taxa, such as *C. neapolitana* and, to a lesser extent, *Leptocythere* species. *Sagmocythere versicolor*, a species preferring sandy pelite bottoms (Frezza & Di Bella, 2015 and references therein), essentially composes the rest of the ostracod assemblage.

Interpretation. For this facies, the mottled texture with local preserved laminae stacked with inverse to normal grading, and up to silt grain size associated with low lignin content and high bioturbation levels, resemble typical fine-grained drift deposits, found in more distal environments and deposited under thermohaline-driven geostrophic contour currents (e.g. Hollister, 1967; Lovell & Stow, 1981; Shanmugam *et al.*, 1993; Stow *et al.*, 1998; Shanmugam, 2000; Martín-Chivelet *et al.*, 2008; Stow & Smillie, 2020; De Castro *et al.*, 2021; Paz *et al.*, 2022). The higher Ni content compared to KS02-357 suggests sediment contribution from the Po River, with subsequent along-shelf sediment transport (Amorosi *et al.*, 2022). Coccolith-bearing mudstone lithics suggest additional sourcing from the carbonate successions of the Gargano Promontory (Morsilli

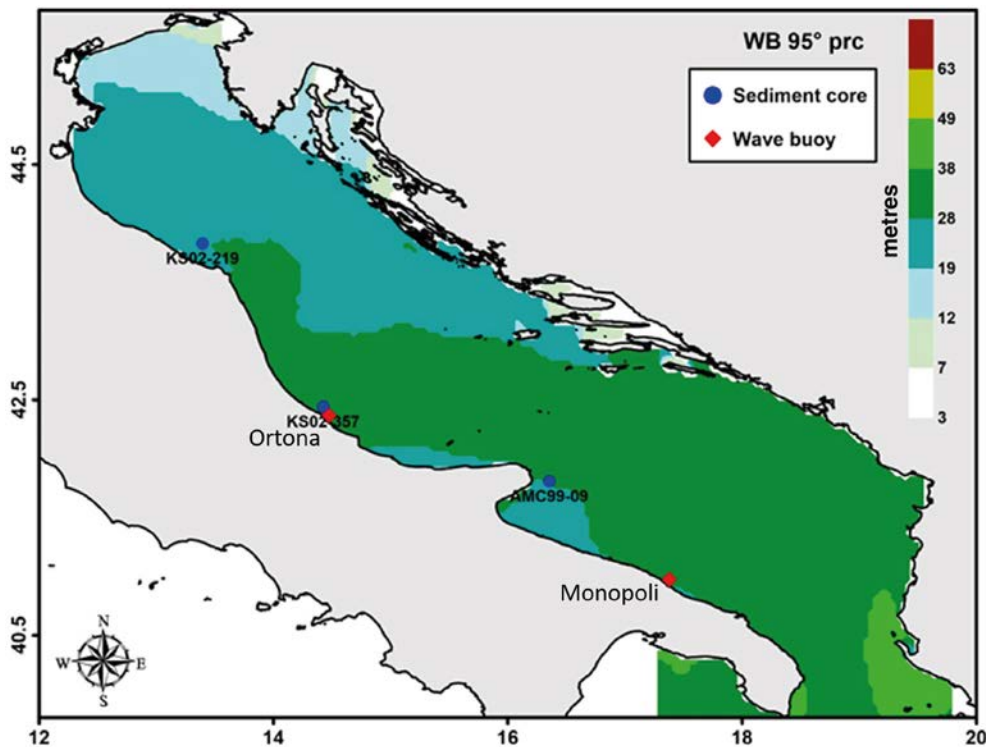


Fig. 12. Estimated wave base from oceanographic data (colour scale, in metres) using median peak periods associated with significant wave heights >95th percentile.

et al., 2004) and possibly from the Northern Apennines (Fiorentino, 1994; Fig. 1), whereas metamorphic fragments were likely derived from the Laga Formation (Chiocchini & Cipriani, 1992). The meiofauna points to a marine setting subject to high to moderate input of OM, with a significant accumulation of fine-grained particles (Frezza & Di Bella, 2015; Rossi *et al.*, 2021). The variety of benthic foraminifer species that includes sensitive and epiphytic taxa suggests modest turbidity and no oxygen deficiency at the sea bottom.

Oceanographic modelling

Figure 12 shows the storm-wave base computed from model data (30-year dataset), which has a dominant north–south gradient, associated with south-easterly winds, and a minor west–east gradient in the northern Adriatic, associated with north-easterly winds. The ‘typical’ storm-wave base is approximately 30 m for all sites in the modern climate (roughly corresponding to waves with 6 s period). This assessment was confirmed using buoy data (in water depths of 31 m, off Ortona, and 35 m, off Monopoli). Considering the water depths where the three study

cores were retrieved, KS02-219, and to a lesser extent AMC99-09, are close to the estimated storm-wave base, whereas KS02-357 appears deeper than the average storm-wave activity (Fig. 12).

DISCUSSION

Lateral heterogeneity of prodelta slope mud deposits: the Little Ice Age stratigraphic unit

Recent sedimentology research in fine-grained deposits has demonstrated that, in many cases, mudstones are not the product of suspension settling, but rather of traction currents that transport flocculated mud and eroded seafloor mud in the form of ‘soft’ clasts (e.g. Schieber *et al.*, 2007, 2010, 2019; Lamb *et al.*, 2008; Bhattacharya & MacEachern, 2009; Schieber & Southard, 2009; Schieber & Yawar, 2009; Macquaker *et al.*, 2010; Schieber, 2011; Plint, 2014; Eide *et al.*, 2018; Schieber & Shao, 2021). the present study shows that the products of sediment transport (beds) in a short-lived (350 years), mud-

dominated system (the LIA unit) investigated over >600 km along-strike reflect a variety of transport mechanisms in a prodelta environment and stack to form highly heterogeneous architectural elements. The LIA unit shows strong lateral variations of the thin-bedded prodelta facies, with: (i) a storm-dominated system in the northern area, passing abruptly into; (ii) a fluvial-dominated system offshore the Pescara River; and (iii) a drift-dominated system governed by along-shelf contour-currents offshore the Gargano Promontory (Fig. 13). The deposition of the LIA unit appears to be forced by the depth of the water column, the steepness of river catchments, the oceanographic conditions on the shelf and by global climate. The following sections examine the main sedimentary patterns and infer controlling factors of prodelta sedimentation in three distinctive sectors of the prodelta slope within the LIA unit.

Storm-dominated system

The storm-dominated system records the interplay between storms (80% of beds) and along-shelf current transport (20% of beds; Fig. 13). The presence of stacked beds with coarser laminae, together with the bimodal nature of BI, suggest an alternation between oscillatory energetic conditions at the seafloor likely reflecting an increased recurrence of storms, as documented in other records for the Mediterranean Sea during the LIA (Camuffo *et al.*, 2000; Sorrel *et al.*, 2012). In this sector, Sirocco winds, owing to the long fetch along the major axis of the Adriatic Sea, can build up rather energetic waves. Bora winds have shorter fetch, but are severe enough to generate energetic waves as well. In both cases, the sea state generated in the coastal area can exert bed shear stresses capable of eroding and re-suspending fine-grained sediment (Fain *et al.*, 2007; Friedrichs & Scully, 2007; Traykovski *et al.*, 2007; Harris *et al.*, 2008). At the same time, geostrophic currents further south in the basin are capable of dispersing sediment along the shelf during river flood events (Cattaneo *et al.*, 2007; Pellegrini *et al.*, 2021). The co-occurrence of benthic species with variable degrees of tolerance to organic enrichment and substrate types points to a muddy plume strongly remobilized by wave currents (Fig. 13), consistent with the inferred depth of the wave base. Regarding shore-parallel sediment transport, the scarcity of lignin indicates that the sediment underwent dispersal, reworking, and redistribution, as documented in

other continental shelf settings (Fig. 12; Allison *et al.*, 2000; Keil *et al.*, 2004; Goni *et al.*, 2008; Zonneveld *et al.*, 2010; Bao *et al.*, 2016, 2019; Bianchi *et al.*, 2018; Bröder *et al.*, 2018; Denomme *et al.*, 2018). Overall, this finding implies that the amount of lignin is not necessarily related to the proximity to river mouths, because reworking and erosion also play a key role (e.g. Bao *et al.*, 2016; Pellegrini *et al.*, 2021). Trace metal distribution reflects hundreds of kilometres of shore parallel transport of Po-derived material (Amorosi *et al.*, 2022), via the south-eastward along-shelf currents. Nickel counts show a sharp increase at the base of the LIA unit and maximum values in its medium/upper portion, suggesting periods with more energetic storm events (Fig. 13). In particular, Bora winds, in addition to generating severe sea states, typically intensify the shore-parallel transport of the WACC (Wang & Pinardi, 2002; Harris *et al.*, 2008). Book *et al.* (2007) reported shore-parallel intense currents (80 cm/s) in the mid-Adriatic in the presence of Bora wind-storms. Moreover, during years of NAdDW generation, the spreading of the new water mass causes a plume of dense shelf water and suspended sediment to extend from the Po River region beyond the Gargano Peninsula, contributing to the overall southward sediment transport and the shore-parallel distribution of muddy shelf deposits (Cattaneo *et al.*, 2003; Palinkas & Nittrouer, 2006; Harris *et al.*, 2008; Pellegrini *et al.*, 2015) and promoting bedsets with >10 km extent, skewed relative to the main river entry points (Fig. 13).

River-dominated system

The river-dominated system mainly records the interplay between river flood events (55% of beds), along-shelf current transport (42% of beds) and minor storm activity (3% of beds; Fig. 13). Stacked, pervasive very fine sand-silty laminae together with a drop in BI suggest high-frequency floods that could be related to an increase in precipitation (Büntgen *et al.*, 2011), an advance of the Apennine glaciers (Giraudi, 2017) or a decrease in tree cover (Oldfield *et al.*, 2003; Kaplan *et al.*, 2009; Giosan *et al.*, 2012; Maselli & Trincardi, 2013; Renaud *et al.*, 2013) that in turn enhanced the sediment yield. The lignin is well-preserved and its presence, coupled with high sediment accumulation rates, indicates rapid burial and stressed bottom conditions (Zonneveld *et al.*, 2010; Bröder *et al.*, 2018; Bao *et al.*, 2019; Pellegrini *et al.*, 2021). The dominance of a poorly-diversified, opportunistic fauna, able to

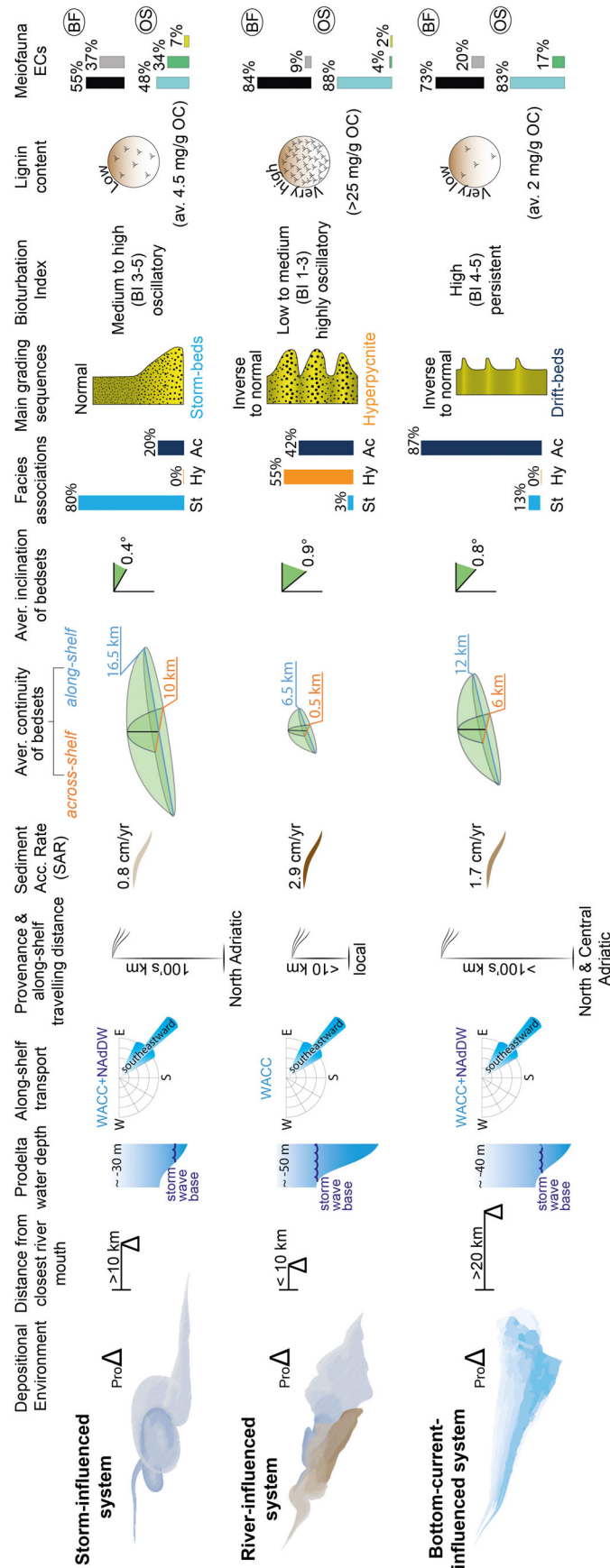


Fig. 13. Schematic representation of the along-strike variability reconstructed from the Little Ice Age (LIA) unit in coalescing prodeltas. Oceanographic conditions of importance to bed character include turbidity, nutrient availability, and dominant energy mode (storm, river, and along-shelf currents). The main Adriatic currents involved are the Western Adriatic Coastal Current (WACC) and the North Adriatic Dense Water (NADW). Facies associations reconstructed include: Storm (St); Hyperpycnite (Hy); and Along-shelf current beds (Ac). Benthic Foraminifera (BF) and Ostracoda (OS) were considered for Meiofauna Ecological Categories (ECs).

thrive on bottoms subject to repeated river fluxes (Van der Zwaan & Jorissen, 1991; Barbieri *et al.*, 2019), further support our interpretation. These beds can be considered analogues of ancient shelf beds with similar sedimentary characteristics, ascribed to river plumes generated during flood episodes (i.e. hyperpycnites, Mutti *et al.*, 2003; Bhattacharya & MacEachern, 2009; Wilson & Schieber, 2014). The storm-wave base indicated by the oceanic model is shallow enough to spare most of the slope of the central Adriatic prodelta from wave reworking, promoting the preservation of river flood deposits that bypassed the shallower sector and deposited in water deeper than 50 m (Fig. 13). In this central sector, the prodelta is dominated by local sediment input, as corroborated by sediment provenance reconstructions (Amorosi *et al.*, 2022). The river-dominated system occupies a sector where the shelf width shrinks to <20 km and shows a prodelta slope of up to 1°, steeper than in the northern sector (Trincardi *et al.*, 2014). This suggests that the physiography of the shelf plays a key role in determining the modes of sediment transport and deposition, promoting the preservation of hyperpycnites in a steeper, though still close to shore, prodelta slope (Fig. 13). During periods of limited river flooding, sediment transport and deposition (29% of beds) appear to reflect near-bed Ekman spirals, where midwater currents flow southward parallel to the bathymetry, as a part of the WACC (Puig *et al.*, 2007). Under these conditions, prodelta deposits result in bedsets that are skewed along the shelf, with strongly reduced (<0.5 km) across-shelf continuity (Fig. 13). The NAdDW in the KS02-357 area generally flows around 90 m or deeper (Sellschopp & Álvarez, 2003; Rice *et al.*, 2013; Marini *et al.*, 2016), thus offshore of the sediment core location.

Drift-dominated system

The drift-dominated system is influenced by along-shelf bottom currents (87% of beds) and storm events (13% of beds; Fig. 13). The inverse to normal grading and persistently high BI are usually found in the contouritic depositional environment (Lovell & Stow, 1981; Stow *et al.*, 1982; Gonthier *et al.*, 1984; Dorador *et al.*, 2019; Yu *et al.*, 2020; Gauchery *et al.*, 2021; Paz *et al.*, 2022). The Adriatic drift-dominated system, however, is located where the shelf is shallower than 100 m and has a prodelta slope of *ca* 0.8° (Trincardi *et al.*, 2014). Because storm waves are still affecting this sector, these strata cannot be interpreted as

contourites in the sense of Hollister (1967), and thus the authors prefer to use the term ‘drift-related beds’ when describing such deposits (Fig. 13). The preserved traction structures were generated during bedload sediment segregation from mixed clay–silt suspensions and consequent formation of floccule silt laminae, similar to flume experiments (Schieber, 2011; Yawar & Schieber, 2017). By looking at similar deposits documented worldwide, the authors wonder if these conditions were also recorded in fossil examples of fine-grained depositional systems that have been interpreted as produced by bottom currents of ‘various nature’, so far (e.g. Pratt, 1984; O’Brien, 1996; Schieber, 1998, 1999, 2016; Loucks & Ruppel, 2007; Singh *et al.*, 2008; Trabuco-Alexandre *et al.*, 2012; Egenhoff & Fishman, 2013; Leonowicz, 2013; Nyhuis *et al.*, 2014; Birgenheier *et al.*, 2017; Li & Schieber, 2018; Minisini *et al.*, 2018). The oceanographic model shows a weak interaction between wave base (at *ca* 40 m water depth) and the prodelta sector (Fig. 12), accounting for the preservation of such drift deposits. Trace metal distribution documents shore-parallel mixing with south-east-directed material sourced from river catchments of the central Apennines, with a discernible, yet minor, contribution of particles from the Po River (Amorosi *et al.*, 2022, 2023) that had to travel for hundreds of kilometres along the shelf (Fig. 13). The proportion of lignin is very low, the lowest encountered in the LIA prodelta slope (Fig. 13), suggesting a depletion of terrestrial organic matter along the transport pathway of sediments on the shelf (Bao *et al.*, 2016, 2019; Bianchi *et al.*, 2018). The low lignin content is thus suggesting a high time interval spent under oxic–suboxic conditions before burial in sediments. Thus, the authors suggest that the low lignin content coupled with inverse to normal grading and high BI can be diagnostic parameters to detect drift-related beds (Fig. 13). The remarkable abundance of a meiofauna with clear opportunistic response to organic enrichment indicates the presence of marine OM, fuelled by the oceanic currents. This agrees with earlier work that documented the prevalence of marine phytoplankton offshore the Gargano Promontory (e.g. Tesi *et al.*, 2007).

The main direction of the oceanic current is south-east, with the WACC and intermittent currents associated with the NAdDW (Sellschopp & Álvarez, 2003; Rice *et al.*, 2013) governing the overall southward sediment transport and the shore-parallel distribution of sediment. Under

these conditions, currents that are able to bypass the central Adriatic shelf can deposit fine-grained sediment south of the Gargano Promontory (Cattaneo *et al.*, 2003; Frignani *et al.*, 2005; Palinkas & Nittrouer, 2006) and form bedsets with >10 km extent, far from a direct river input (Fig. 13). Regarding the shore-parallel sediment transport, it can be also speculated that the WACC might have been reinforced by intensification of the NAdDW during intervals of cooler climatic conditions, such as the Little Ice Age, which resulted in more severe conditions in the North Adriatic (Camuffo *et al.*, 2000). These climate conditions may have enhanced the formation of NAdDW and, concurrently, its ability to impinge along the Adriatic shelf. Drift-dominated deposits constitute an additional example on the growing list of fine-grained successions where traction structures are considered the product of bottom current reworking (e.g. Pratt, 1984; O'Brien, 1996; Schieber, 1998, 1999, 2016; Singh *et al.*, 2008; Trabuco-Alexandre *et al.*, 2012; Frébourg *et al.*, 2013; Leonowicz, 2013; Nyhuis *et al.*, 2014; Birgenheier *et al.*, 2017; Ayranci *et al.*, 2018; Li & Schieber, 2018; Minisini *et al.*, 2018).

Use of sediment archives to decipher palaeoflood frequency

Deposition and preservation of flood deposits in a prodelta environment are controlled by a variety of factors, including: (i) available accommodation (i.e. water depth); (ii) distance from the river mouth; (iii) sediment accumulation rate; and (iv) the stochastic succession of flood events *versus* the recurrence of resuspension processes (e.g. Drexler & Nittrouer, 2008). The sediment accumulation rate, in turn, is largely controlled by the rate of sediment delivery, which varies with the type and scale of rivers (Milliman & Syvitski, 1992; Mulder *et al.*, 2003; Mutti *et al.*, 2003). It is also well-known that rivers do not discharge sediment at a constant rate and that river flood deposits can be easily reworked by later storms (e.g. Friedrichs & Wright, 2004; Dail *et al.*, 2007; Traykovski *et al.*, 2007; Goni *et al.*, 2008; Ogston *et al.*, 2008; Walsh & Nittrouer, 2009).

Massive sediment-discharge events typically occur on only a few days per year (Syvitski *et al.*, 2000; Morehead *et al.*, 2003) and the frequency of flooding also varies with the climate regime (e.g. Piva *et al.*, 2008; Fanget *et al.*, 2014; Pellegrini *et al.*, 2017, 2021). Where individual events record deposition directly from river

plumes, such as in the case of hyperpycnites and turbidites, storm reworking is negligible. Offshore the Pescara River mouth, deposition extends offshore below the storm-wave base, where the preservation potential is higher (Fig. 12).

Prodelta slopes are the potential sites where decadal to century-scale records of river floods can be preserved. The prodeltaic facies described offshore the Pescara River exemplifies the high-fidelity nature of these stratigraphic records, as indicated by numerous hyperpycnal beds associated with limited bioturbation intensity and high lignin content, and preserved below the storm-wave base (Fig. 13). Counting of individual beds in the prodelta of the central sector yielded 41 flooding events in 350 years (Fig. 8), with a *ca* 10 year return interval. This observation suggests an order of magnitude increase of precipitation during the Little Ice Age compared to modern times, enabling rivers to cross the discharge threshold (40 kg/m³) of sediment concentration necessary to overcome the freshwater versus ocean water density contrast (Mulder & Syvitski, 1995; Parsons *et al.*, 2001) and generate hyperpycnal flows.

The 10 year flood recurrence period obtained from the LIA stratigraphic unit is of higher-frequency than the 25 to 50 year recurrence interval predicted by hydrodynamic models for the same region (Syvitski *et al.*, 2000). This observation supports the idea that vertical facies successions from river-dominated prodeltas may contain a reasonably complete record of river flood events, excellent in reconstructing past precipitation histories.

Along-strike facies variability and facies models

Facies models, designed to integrate large and complex sets of observations, and to illuminate underlying processes and external controls, are an indispensable element of the sedimentary geologist's toolbox. Their inherent simplifications, however, while useful for developing an initial framework of environmental interpretation, can be 'dangerous' if applied too literally in the interpretation of facies patterns (Reading, 2001).

Along-strike facies development tends to be less predictable than facies relations reconstructed along-dip, as has been well-illustrated from deltaic (Bhattacharya & Walker, 1991; Bhattacharya, 2006; Olariu & Bhattacharya, 2006; Gani & Bhattacharya, 2007; Li *et al.*, 2015; Rossi

et al., 2017; Peng et al., 2022), shoreface (Rodríguez et al., 2004; Isla et al., 2023), shallow-marine (Eide et al., 2018; Isla et al., 2018; Schwarz et al., 2018) and fluvial (Rittersbacher et al., 2014) successions, as well as from other depositional settings (Poyatos-Moré et al., 2019; Schwarz et al., 2021; Li & Schieber, 2022).

Sedimentation may occur relatively close to the river mouth (Walsh & Nittrouer, 2009), such as in river-dominated delta systems, and there is increasing recognition that small rivers that drain mountainous areas can deliver sediment directly onto the shelf via hyperpycnal flows when they experience flood conditions (Mulder & Syvitski, 1995; Parsons et al., 2001; Mulder et al., 2003; Dadson et al., 2005; Bhattacharya & MacEachern, 2009; Olariu et al., 2010; Zavala et al., 2011; Li et al., 2015; Pellegrini et al., 2021). Sediment gravity flows, such as turbidity currents and fluid muds, are additional mechanisms that can transfer sediment to the shelf and deep water (Ogston et al., 2008; Friedrichs & Wright, 2004; Traykovski et al., 2007). In addition, a variety of shelf processes (chiefly waves, tides and oceanic currents) can transport significant amounts of sediment far from the point of fluvial entry to seaward areas (Cattaneo et al., 2007; Hill et al., 2007; Walsh & Nittrouer, 2009; Pellegrini et al., 2015; Patruno & Helland-Hansen, 2018; Slooman & Cartigny, 2020).

This study illustrates the challenges one faces when trying to project the complex lateral facies variability of the subaqueous delta clinoforms of the West Adriatic LIA deposits into the rock record. Although the LIA stratigraphic unit is a short-lived (350 year), fine-grained clinotherm that could barely be resolved in the rock record, it reflects the influence of distinctive, simultaneously operating controlling factors, pointing to a high degree of spatial and temporal heterogeneity (Fig. 13). The distance from the river mouth to the associated prodelta slope plays a key role in determining the extent to which the oceanographic regime may interact with river-borne sediment. In the LIA unit, prodelta slope deposits show an along-strike reduction of storm event beds to <3%, as the distance from the river mouth decreases. Concurrently, a greater preservation of fluvial-driven event beds (up to 55%) is observed in prodelta slope strata closer to the river mouth (<10 km, for example, Pescara River; Fig. 13), even if the sediment core was located a long-distance downdrift from a big river (for example, the Po River; Fig. 13). This

suggests greater preservation of hyperpycnal deposits in the steeper prodelta slope, where water depths exceeding the 30 m storm-wave base preclude the development of storm facies (Fig. 13).

On the other hand, prodelta slope deposits with dominant storm-generated facies can be preserved close to the river mouth (<20 km, for example, Misa River) if they developed in relatively shallow water (dependent on storm-wave base; Fig. 13). The picture is further complicated by the presence of along-shelf currents that may affect the entire prodelta slope, even in storm and river dominated systems (especially during time intervals of river and storm quiescence, as suggested by higher BI values; Fig. 13), and in prodelta slopes that are a far distance downdrift from the river mouth (more than hundreds of kilometres from the river mouth). Here, drift-related facies, resemble those encountered in contourite deposits, highlighting the importance of characterizing faunal assemblages to avoid errors in inferring palaeo water depths when evaluating outcrop analogues.

The study of modern depositional systems and sedimentary successions, thus, can enable the development of increasingly complex facies models that, as such, may allow to fine-tune the study of ancient successions.

CONCLUSION

A line-sourced prodelta system in the Adriatic epicontinental sea has been used to infer the key processes that governed particle transport and deposition at the bed scale, shaping facies and internal architecture of a fine-grained unit that accumulated over just *ca* 350 years, during the Little Ice Age. This unit is bounded by seismic reflectors (flooding surfaces) that can be traced over several hundreds of kilometres. Inside this unit, processes such as storm surges, river floods, and along-shelf currents are recorded in different proportions along the prodelta slopes. Individual strata record lateral changes in sedimentary structures, sediment provenance, lignin preservation, bioturbation, and oxygen availability, documenting the simultaneous combination of different processes on centennial timescales. Our findings suggest that an apparently homogenous, hundreds of kilometres long, stratigraphic unit accumulated in a few centuries is, instead, much more heterogeneous than expected: sedimentary facies present

substantial differences along-strike as a function of changes in the dominant processes of transport and deposition.

Our results show that: (i) the prodelta slope dominated by storms (for example, Misa River) hosts bedsets with across-shelf continuity of tens of kilometres, upper fine sand beds with erosional basal surface, intermediate values of lignin content, high Ni content recording relatively high shore-parallel sediment transport, systematic variations of the bioturbation index, and a diversified benthic fauna composed of taxa with different degrees of tolerance to organic enrichment; (ii) the prodelta slope dominated by river floods (for example, Pescara River) shows the maximum complexity of stratal geometries, with short-distance bedset terminations and reduced (<1 km) across-shelf bedset continuity, inverse to normal grading, the highest lignin content, as well as the lowest Ni content (i.e. maximum local river supply), and benthic fauna tolerant to high organic matter (OM) fluxes and oxygen deficiency; and (iii) the prodelta sector far from direct river input (off-shore Gargano Promontory) holds bedsets with tens of kilometres across-shelf continuity, inverse to normal grading coupled with low lignin content, high Ni content and high bioturbation index, and benthic fauna typical of high to moderate marine OM fluxes.

This study demonstrates that coalescing prodeltas can show significant variability with regard to terrestrial organic carbon sequestration. The only sector of the prodelta slope that appears efficient in lignin sequestration is that influenced by instantaneous deposition and rapid burial associated with river flood (hyperpycnal) events below storm-wave base. These heterolithic prodelta deposits potentially contain high-fidelity records of river flood events that may be useful for the reconstruction of the frequency and intensity of past precipitation.

ACKNOWLEDGEMENTS

This contribution is part of PRIN-MIUR project “The Po-Adriatic Source-to-Sink system (PASS): from modern sedimentary processes to millennial-scale stratigraphic architecture”, contract 2017ASZAKJ_001. Editors Kevin Taylor and Gabriela Mángano, and Reviewers Ernesto Schwarz and Zhiyang Li are thanked for insightful comments that improved the paper. We thank Alessandra Asioli (CNR-ISMAR) for the useful

discussion that improved the quality of the manuscript.

DATA AVAILABILITY STATEMENT

The data that support the findings of this study are available from the corresponding author upon reasonable request.

REFERENCES

- Aiello, G., Amato, V., Barra, D., Caporaso, L., Caruso, T., Giaccio, B., Parisi, R. and Rossi, A. (2020) Late Quaternary benthic foraminiferal and ostracod response to palaeoenvironmental changes in a Mediterranean coastal area, Port of Salerno, Tyrrhenian Sea. *Reg. Stud. Mar. Sci.*, **40**, 101498.
- Ainsworth, R.B., Vakarelov, B.K. and Nanson, R.A. (2011) Dynamic spatial and temporal prediction of changes in depositional processes on clastic shorelines: toward improved subsurface uncertainty reduction and management. *AAPG Bull.*, **95**(2), 267–297.
- Allison, M.A., Kineke, G.C., Gordon, E.S. and Goni, M.A. (2000) Development and reworking of a seasonal flood deposit on the inner continental shelf off the Atchafalaya River. *Cont. Shelf Res.*, **20**(16), 2267–2294.
- Amorosi, A. and Sammartino, I. (2007) Influence of sediment provenance on background values of potentially toxic metals from near-surface sediments of Po coastal plain (Italy). *Int. J. Earth Sci.*, **96**, 389–396.
- Amorosi, A., Centineo, M.C., Dinelli, E., Lucchini, F. and Tateo, F. (2002) Geochemical and mineralogical variations as indicators of provenance changes in Late Quaternary deposits of SE Po Plain. *Sed. Geol.*, **151**, 273–292.
- Amorosi, A., Guermandi, M., Marchi, N. and Sammartino, I. (2014) Fingerprinting sedimentary and soil units by their natural metal contents: A new approach to assess metal contamination. *Sci. Total Environ.*, **500–501**, 361–372.
- Amorosi, A., Maselli, V. and Trincardi, F. (2016) Onshore to offshore anatomy of a late Quaternary source-to-sink system (Po Plain–Adriatic Sea, Italy). *Earth-Sci. Rev.*, **153**, 212–237.
- Amorosi, A., Sammartino, I., Dinelli, E., Campo, B., Guercia, T., Trincardi, F. and Pellegrini, C. (2022) Provenance and sediment dispersal in the Po-Adriatic source-to-sink system unraveled by bulk-sediment geochemistry and its linkage to catchment geology. *Earth-Sci. Rev.*, **234**, 104202.
- Amorosi, A., Bruno, L., Caldara, M., Campo, B., Cau, S., De Santis, V., Di Martino, A., Hong, W., Lucci, G., Pellegrini, C., Rossi, V. and Vaiani, S.C. (2023) Late Quaternary sedimentary record of estuarine incised-valley filling and interfluvial flooding: The Manfredonia paleovalley system (southern Italy). *Mar. Pet. Geol.*, **147**, 105975.
- Anell, I., Olsen, S.G., Haugen, M., Jahren, J., Midtkandal, I. and Poyatos-Moré, M. (2023) A discourse on factors influencing the formation of sigmoidal and linear slope-geometries in the deltaic clinoforms of the calciclastic Sobrarbe Delta, Ainsa Basin, Spain. *Mar. Petrol. Geol.*, **153**, 106287.

- Arnott, R.W. and Southard, J.B.** (1990) Exploratory flow-duct experiments on combined-flow bed configurations, and some implications for interpreting storm-event stratification. *J. Sediment. Res.*, **60**(2), 211–219.
- Ayranci, K., Harris, N.B. and Dong, T.** (2018) Sedimentological and ichnological characterization of the Middle to Upper Devonian Horn River Group, British Columbia, Canada: Insights into mudstone depositional conditions and processes below storm wave base. *J. Sed. Res.*, **88**, 1–23.
- Bao, R., McIntyre, C., Zhao, M., Zhu, C., Kao, S.J. and Eglinton, T.I.** (2016) Widespread dispersal and aging of organic carbon in shallow marginal seas. *Geology*, **44**, 791–794.
- Bao, R., Zhao, M., McNichol, A., Wu, Y., Guo, X., Haghipour, N. and Eglinton, T.I.** (2019) On the origin of aged sedimentary organic matter along a river-shelf-deep ocean transect. *J. Geophys. Res. Biogeosci.*, **124**(8), 2582–2594.
- Barbieri, G., Rossi, V., Vaiani, S.C. and Horton, B.P.** (2019) Benthic ostracoda and foraminifera from the North Adriatic Sea (Italy, Mediterranean Sea): A proxy for the depositional characterisation of river-influenced shelves. *Mar. Micropaleontol.*, **153**, 101772.
- Benetazzo, A., Bergamasco, A., Bonaldo, D., Falcieri, F.M., Sclavo, M., Langone, L. and Carniel, S.** (2014) Response of the Adriatic Sea to an intense cold air outbreak: dense water dynamics and wave-induced transport. *Prog. Oceanogr.*, **128**, 115–138.
- Bentley, S.J. and Nittrouer, C.A.** (2003) Emplacement, modification, and preservation of event strata on a flood-dominated continental shelf: Eel shelf, Northern California. *Cont. Shelf Res.*, **23**(16), 1465–1493.
- Bentley, S.J., Blum, M.D., Maloney, J., Pond, L. and Paulsell, R.** (2016) The Mississippi River source-to-sink system: Perspectives on tectonic, climatic, and anthropogenic influences, Miocene to Anthropocene. *Earth-Sci. Rev.*, **153**, 139–174.
- Berner, R.** (1981) A new geochemical classification of sedimentary environments. *J. Sediment. Petrol.*, **51**, 359–365.
- Berner, R.A., VandenBrooks, J.M. and Ward, P.D.** (2007) Oxygen and evolution. *Science*, **316**(5824), 557–558.
- Bhattacharya, J.P.** (2006) Deltas. In: *Facies Models Revised* (Eds Posamentier, H.W. and Walker, R.G.), *SEPM Spec. Publ.*, **84**, 237–292. ISBN 1-56576-121-9.
- Bhattacharya, J.P. and MacEachern, J.A.** (2009) Hyperpycnal rivers and prodeltaic shelves in the Cretaceous seaway of North America. *J. Sed. Res.*, **79**(4), 184–209.
- Bhattacharya, J.P., Howell, C.D., MacEachern, J.A. and Walsh, J.P.** (2020) Bioturbation, sedimentation rates, and preservation of flood events in deltas. *Palaeogeogr. Palaeoclimatol. Palaeoecol.*, **560**, 110049.
- Bhattacharya, J.P. and Walker, R.G.** (1991) River- and wave-dominated depositional systems of the Upper Cretaceous Dunvegan Formation, northwestern Alberta. *Bull. Can. Pet. Geol.*, **39**, 165–191.
- Bianchi, T.S., Cui, X., Blair, N.E., Burdige, D.J., Eglinton, T.I. and Galy, V.** (2018) Centers of organic carbon burial and oxidation at the land-ocean interface. *Org. Geochem.*, **115**, 138–155.
- Birgenheier, L.P., Horton, B., McCauley, A.D., Johnson, C.L. and Kennedy, A.** (2017) A depositional model for offshore deposits of the lower Blue Gate Member, Mancos Shale, Uinta Basin, Utah, USA. *Sedimentology*, **64**, 1402–1438.
- Blair, N.E., Leithold, E.L. and Aller, R.C.** (2004) From bedrock to burial: the evolution of particulate organic carbon across coupled watershed-continental margin systems. *Mar. Chem.*, **92**, 141–156.
- Bohacs, K.M., Lazar, O.R. and Demko, T.M.** (2014) Parasequence types in shelfal mudstone strata—Quantitative observations of lithofacies and stacking patterns, and conceptual link to modern depositional regimes. *Geology*, **42**, 131–134.
- Bonaduce, G., Ciampo, G. and Masoli, M.** (1975) Distribution of Ostracoda in the Adriatic Sea. *Pubblicazioni della Stazione Zoologica di Napoli*, **40**, 304.
- Bond, G., Showers, W., Cheseby, M., Lotti, R., Almasi, P., Priore, P., Cullen, H., Hajdas, I. and Bonani, G.** (1997) A pervasive millennial-scale cycle in North Atlantic Holocene and glacial climates. *Science*, **278**, 1257–1266.
- Bond, G., Kromer, B., Beer, J., Muscheler, R., Evans, M.N., Showers, W., Hoffmann, S., Lotti-Bond, R., Hajdas, I. and Bonani, G.** (2001) Persistent solar influence on North Atlantic climate during the Holocene. *Science*, **294**, 2130–2136.
- Book, J.W., Signell, R.P. and Perkins, H.** (2007) Measurements of storm and nonstorm circulation in the northern Adriatic: October 2002 through April 2003. *J. Geophys. Res. Oceans*, **112**(C11), 3556.
- Boulesteix, K., Poyatos-Moré, M., Flint, S.S., Taylor, K.G., Hodgson, D.M. and Hasiotis, S.T.** (2019) Transport and deposition of mud in deep-water environments: Processes and stratigraphic implications. *Sedimentology*, **66**(7), 2894–2925.
- Bradley, R.S. and Jonest, P.D.** (1993) ‘Little Ice Age’ summer temperature variations: their nature and relevance to recent global warming trends. *Holocene*, **3**(4), 367–376.
- Breman, E.** (1975) *The distribution of ostracodes in the bottom sediments of the Adriatic Sea*. PhD Thesis. Vrije Universiteit, Amsterdam.
- Brett, C.E. and Allison, P.A.** (1998) Paleontological approaches to the environmental interpretation of marine mudrocks. In: *Shales and Mudstones* (Eds Schieber, J., Zimmerle, W. and Sethi, P.), pp. 301–349. Schweizerbart, Stuttgart.
- Bröder, L., Tesi, T., Andersson, A., Semiletov, I. and Gustafsson, Ö.** (2018) Bounding cross-shelf transport time and degradation in Siberian-Arctic land-ocean carbon transfer. *Nat. Commun.*, **9**(1), 806.
- Büntgen, U., Tegel, W., Nicolussi, K., McCormick, M., Frank, D., Trouet, V. and Esper, J.** (2011) 2500 years of European climate variability and human susceptibility. *Science*, **331**(6017), 578–582.
- Campbell, C.V.** (1967) Lamina, laminaset, bed, and bedset. *Sedimentology*, **8**, 7–26.
- Campbell, I.D., Campbell, C., Apps, M.J., Rutter, N.W. and Bush, A.B.G.** (1998) Late Holocene ~1500 yr climatic periodicities and their implications. *Geology*, **26**, 471–473.
- Camuffo, D., Secco, C., Brimblecombe, P. and Martin-Vide, J.** (2000) Sea storms in the Adriatic Sea and the Western Mediterranean during the last millennium. *Clim. Change*, **46**(1), 209–223.
- de Castro, S., Miramontes, E., Dorador, J., Jouet, G., Cattaneo, A., Rodríguez-Tovar, F.J. and Hernández-Molina, F.J.** (2021) Siliciclastic and bioclastic contouritic sands: Textural and geochemical characterisation. *Mar. Pet. Geol.*, **128**, 105002.
- Cattaneo, A., Correggiari, A., Langone, L. and Trincardi, F.** (2003) The late-Holocene Gargano subaqueous delta,

- Adriatic shelf: sediment pathways and supply fluctuations. *Mar. Geol.*, **193**, 61–91.
- Cattaneo, A., Trincardi, F., Langone, L., Asioli, A. and Puig, P. (2004) Clinoform generation on Mediterranean margins. *Oceanography*, **17**(4), 104–117.
- Cattaneo, A., Trincardi, F., Asioli, A. and Correggiari, A. (2007) The western Adriatic shelf clinoform: energy-limited bottomset. *Cont. Shelf Res.*, **27**, 506–525.
- Chen, F., Zhu, X.Y., Wang, W., Wang, F., Hieu, P.T. and Siebel, W. (2009) Single-grain detrital muscovite Rb-Sr isotopic composition as an indicator of provenance for the Carboniferous sedimentary rocks in northern Dabie, China. *Geochim. J.*, **43**(4), 257–273.
- Chiggiato, J., Bergamasco, A., Borghini, M., Falcieri, F.M., Falco, P., Langone, L., Miserocchi, S., Russo, A. and Schroeder, K. (2016) Dense-water bottom currents in the Southern Adriatic Sea in spring 2012. *Mar. Geol.*, **375**, 134–145.
- Chiocchini, U. and Cipriani, N. (1992) Provenance and evolution of Miocene turbidite sedimentation in the central Apennines, Italy. *Sed. Geol.*, **77**(3–4), 185–195.
- Collins, D.S., Johnson, H.D., Allison, P.A., Guilpain, P. and Damit, A.R. (2017) Coupled ‘storm-flood’ depositional model: Application to the Miocene–Modern Baram Delta Province, north-west Borneo. *Sedimentology*, **64**(5), 1203–1235.
- Correggiari, A., Cattaneo, A. and Trincardi, F. (2005) Depositional patterns in the Late-Holocene Po delta system. In: *River Deltas: Concepts Models and Examples* (Eds Bhattacharya, J.P. and Giosan, L.), *SEPM Spec Publ*, **83**, 365–392.
- Crowley, T.J. (2000) Causes of climatic change over the past 1000 years. *Science*, **289**, 270–277.
- Cushman-Roisin, B. and Naimie, C.E. (2002) A 3D finite-element model of the Adriatic tides. *J. Mar. Syst.*, **37**, 279–297.
- Dadson, S., Hovius, N., Pegg, S., Dade, W.B., Horng, M.J. and Chen, H. (2005) Hyperpycnal river flows from an active mountain belt. *J. Geophys. Res. Earth Surf.*, **110**, F04016.
- Dail, M.B., Corbett, D.R. and Walsh, J.P. (2007) Assessing the importance of tropical cyclones on continental margin sedimentation in the Mississippi delta region. *Continental Shelf Res.*, **27**(14), 1857–1874.
- Denommee, K.C., Bentley, S.J. and Harazim, D. (2018) Mechanisms of muddy clinothem progradation on the Southwest Louisiana Chenier Plain inner shelf. *Geo-Mar. Lett.*, **38**(3), 273–285.
- Dorador, J., Rodriguez-Tovar, F.J., Mena, A. and Francés, G. (2019) Lateral variability of ichnological content in muddy contourites: Weak bottom currents affecting organisms’ behavior. *Sci. Rep.*, **9**(1), 17713.
- Drexler, T.M. and Nittrouer, C.A. (2008) Stratigraphic signatures due to flood deposition near the Rhône River: Gulf of Lions, northwest Mediterranean Sea. *Cont. Shelf Res.*, **28**, 1877–1894.
- Dypvik, H. and Harris, N.B. (2001) Geochemical facies analysis of fine-grained siliciclastics using Th/U, Zr/Rb and (Zr+ Rb)/Sr ratios. *Chem. Geol.*, **181**(1–4), 131–146.
- Egenhoff, S.O. and Fishman, N.S. (2013) Traces in the dark —Sedimentary processes and facies gradients in the upper shale member of the Upper Devonian–Lower Mississippian Bakken Formation, Williston Basin, North Dakota, USA. *J. Sed. Res.*, **83**(9), 803–824.
- Eide, C.H., Klausen, T.G., Katkov, D., Suslova, A.A. and Helland-Hansen, W. (2018) Linking an Early Triassic delta to antecedent topography: Source-to-sink study of the southwestern Barents. *Sea Margin. Bull.*, **130**(1–2), 263–283.
- Fain, A.M.V., Ogston, A.S. and Sternberg, R.W. (2007) Sediment transport event analysis on the western Adriatic continental shelf. *Cont. Shelf Res.*, **27**, 431–451.
- Fanget, A.S., Berné, S., Jouet, G., Bassetti, M.A., Dennielou, B., Maillet, G.M. and Tondut, M. (2014) Impact of relative sea level and rapid climate changes on the architecture and lithofacies of the Holocene Rhone subaqueous delta (Western Mediterranean Sea). *Sed. Geol.*, **305**, 35–53.
- Fiorentino, A. (1994) I nannofossili e la biostratigrafia dell’Appennino centrale: generalità e applicazioni. In: *Biostratigrafia dell’Italia centrale* (Ed. Farinacci, A.), *Studi Geologici Camerti*, **8**, 131–155.
- Fiorini, F. and Vaiani, S.C. (2001) Benthic foraminifers and transgressive-regressive cycles in the Late Quaternary subsurface sediments of the Po Plain near Ravenna (Northern Italy). *Boll. Soc. Paleontol. Italy*, **40**, 357–403.
- Foglini, F., Campiani, E. and Trincardi, F. (2016) The reshaping of the South West Adriatic Margin by cascading of dense shelf waters. *Marine Geol.*, **375**, 64–81.
- Fonnesu, M. and Felletti, F. (2019) Facies and architecture of a sand-rich turbidite system in an evolving collisional-trench basin: a case history from the Upper Cretaceous–Palaeocene Gottero system (NW Apennines). *Riv. It. Paleontol. Strat.*, **125**(2), 449–487.
- Foukal, P., North, G. and Wigley, T. (2004) A stellar view on solar variations and climate. *Science*, **306**, 68–69.
- Frébourg, G., Ruppel, S.C. and Rowe, H. (2013) Sedimentology of the Haynesville (Upper Kimmeridgian) and Bossier (Tithonian) Formations, in the Western Haynesville Basin, Texas, USA. *AAPG Memoir*, **105**, 47–67.
- Frezza, V. and Carboni, M.G. (2009) Distribution of recent foraminiferal assemblages near the Ombrone River mouth (Northern Tyrrhenian Sea, Italy). *Revue de micropaléontologie*, **52**(1), 43–66.
- Frezza, V. and Di Bella, L. (2015) Distribution of recent ostracods near the Ombrone River mouth (Northern Tyrrhenian Sea, Italy). *Micropaleontology*, **61**, 101–114.
- Friedrichs, C.T. and Scully, M.E. (2007) Modeling deposition by wave-supported gravity flows on the Po River prodelta: from seasonal floods to prograding clinoforms. *Cont. Shelf Res.*, **27**(3–4), 322–337.
- Friedrichs, C.T. and Wright, L.D. (2004) Gravity-driven sediment transport on the continental shelf: implications for equilibrium profiles near river mouths. *Coast. Eng.*, **51** (8–9), 795–811.
- Frignani, M., Langone, L., Ravaioli, M., Sorgente, D., Alvisi, F. and Albertazzi, S. (2005) Fine sediment mass balance in the western Adriatic continental shelf over a century time scale. *Mar. Geol.*, **222–223**, 113–133.
- Gani, M.R. and Bhattacharya, J.P. (2007) Basic building blocks and process variability of a Cretaceous delta: internal facies architecture reveals a more dynamic interaction of river, wave, and tidal processes than is indicated by external shape. *J. Sed. Res.*, **77**(4), 284–302.
- Garzanti, E., Resentini, A., Vezzoli, G., Ando, S., Malusa, M.G., Padoan, M. and Paparella, P. (2010) Detrital fingerprints of fossil continental-subduction zones (Axial Belt Provenance, European Alps). *J. Geol.*, **118**, 341–362.
- Gauchery, T., Rovere, M., Pellegrini, C., Asioli, A., Tesi, T., Cattaneo, A. and Trincardi, F. (2021) Post-LGM multiproxy sedimentary record of bottom-current variability and

- downslope sedimentary processes in a contourite drift of the Gela Basin (Strait of Sicily). *Mar. Geol.*, **439**, 106564.
- Giosan, L., Coolen, M.J., Kaplan, J.O., Constantinescu, S., Filip, F., Filipova-Marinova, M. and Thom, N. (2012) Early anthropogenic transformation of the Danube-Black Sea system. *Sci. Rep.*, **2**, 582.
- Giraudi, C. (2017) Climate evolution and forcing during the last 40 ka from the oscillations in Apennine glaciers and high mountain lakes, Italy. *J. Quatern. Sci.*, **32**(8), 1085–1098.
- Glaser, R., Riemann, D., Schönbein, J., Barriendos, M., Brázdil, R., Bertolin, C. and Himmelsbach, I. (2010) The variability of European floods since AD 1500. *Clim. Change*, **101**(1), 235–256.
- Goineau, A., Fontanier, C., Mojtahid, M., Fanget, A.S., Bassetti, M.A., Berné, S. and Jorissen, F. (2015) Live–dead comparison of benthic foraminiferal faunas from the Rhône prodelta (Gulf of Lions, NW Mediterranean): Development of a proxy for palaeoenvironmental reconstructions. *Mar. Micropaleontol.*, **119**, 17–33.
- Goni, M.A., Monacchi, N., Gisewhite, R., Crockett, J., Nittrouer, C., Ogston, A., Simone, R.A. and Aalto, R. (2008) Terrigenous organic matter in sediments from the Fly River delta-clinoform system (Papua New Guinea). *J. Geophys. Res. Earth Surf.*, **113**(F1), 653.
- Gonthier, E.G., Faugères, J.C. and Stow, D.A.V. (1984) Contourite facies of the Faro drift, Gulf of Cadiz. *Geol. Soc. Spec. Publ.*, **15**(1), 275–292.
- Goodbred, S.L., Kuehl, S.A., Steckler, M. and Sarker, M.H. (2003) Controls on facies distribution and stratigraphic preservation in the Ganges–Brahmaputra delta sequence. *Sed. Geol.*, **155**, 301–316.
- Gordon, E.S. and Goñi, M.A. (2003) Sources and distribution of terrigenous organic matter delivered by the Atchafalaya River to sediments in the northern Gulf of Mexico. *Geochim. Cosmochim. Acta*, **67**(13), 2359–2375.
- Grundvåg, S.A., Jelby, M.E., Olausson, S. and Śliwińska, K.K. (2021) The role of shelf morphology on storm-bed variability and stratigraphic architecture, Lower Cretaceous, Svalbard. *Sedimentology*, **68**(1), 196–237.
- Hage, S., Romans, B.W., Peplow, T.G., Poyatos-Moré, M., Haeri Ardakani, O., Bell, D. and Hubbard, S.M. (2022) High rates of organic carbon burial in submarine deltas maintained on geological timescales. *Nat. Geosci.*, **15**(11), 1–6.
- Harris, C.K., Sherwood, C.R., Signell, R.P., Bever, A.J. and Warner, J.C. (2008) Sediment dispersal in the northwestern Adriatic Sea. *J. Geophys. Res. Oceans*, **113**(C11), 3868.
- Hedges, J.I., Keil, R.G. and Benner, R. (1997) What happens to terrestrial organic matter in the ocean? *Org. Geochem.*, **27**, 195–212.
- Hill, P.S., Fox, J.M., Crockett, J.S., Curran, K.J., Friedrichs, C.T., Geyer, W.R., Syvitski, J.P. and Wheatcroft, R.A. (2007) Sediment delivery to the seabed on continental margins. In: *Continental Margin Sedimentation: From Sediment Transport to Sequence Stratigraphy* (Eds Nittrouer, C.A., Austin, J.A., Field, M.E., Kravitz, J.H., Syvitski, J.P.M. and Wiberg, P.L.), *Spec. Publ.*, **37**, 49–99.
- Hollister, C.D. (1967) *Sediment distribution and deep circulation in the western North Atlantic*. PhD dissertation. Columbia University, New York, NY, 467 pp.
- Holzhauser, H., Magny, M. and Zumbühl, H.J. (2005) Glacier and lake-level variations in west-central Europe over the last 3500 years. *Holocene*, **15**(6), 789–801.
- Isla, M.F., Schwarz, E. and Veiga, G.D. (2018) Bedset characterization within a wave-dominated shallow-marine succession: an evolutionary model related to sediment imbalances. *Sed. Geol.*, **374**, 36–52.
- Isla, M.F., Moyano-Paz, D., FitzGerald, D.M., Simontacchi, L. and Veiga, G.D. (2023) Contrasting beach-ridge systems in different types of coastal settings. *Earth Surf. Process. Landf.*, **48**, 47–71.
- Jalali, B., Sicre, M.A., Klein, V., Schmidt, S., Maselli, V., Lirer, F. and Châles, F. (2018) Deltaic and coastal sediments as recorders of Mediterranean regional climate and human impact over the past three millennia. *Paleoceanogr. Paleoclimatol.*, **33**(6), 579–593.
- Jaramillo, S., Sheremet, A., Allison, M.A., Reed, A.H. and Holland, K.T. (2009) Wave-mud interactions over the muddy Atchafalaya subaqueous clinoform, Louisiana, United States: Wave-supported sediment transport. *J. Geophys. Res. Oceans*, **114**(C4), 4821.
- Jerolmack, D.J. and Paola, C. (2010) Shredding of environmental signals by sediment transport. *Geophys. Res. Lett.*, **37**(19), 44638.
- Jones, P.D. and Mann, M.E. (2004) Climate over past millennia. *Rev. Geophys.*, **42**, RG2002.
- Jorissen, F.J. (1988) Benthic foraminifera from the Adriatic Sea; principles of phenotypic variation. *Utrecht Micropaleontol. Bull.*, **37**, 1–176.
- Jorissen, F.J., Nardelli, M.P., Almogi-Labin, A., Barras, C., Bergamin, L., Bicchi, E., El Kateb, A., Ferraro, L., McGann, M., Morigi, C., Romano, E., Sabbatini, A., Schweizer, M. and Spezzaferri, S. (2018) Developing Foram-AMBI for biomonitoring in the Mediterranean: species assignments to ecological categories. *Mar. Micropaleontol.*, **140**, 33–45.
- Kaplan, J.O., Krumhardt, K.M. and Zimmermann, N. (2009) The prehistoric and preindustrial deforestation of Europe. *Quat. Sci. Rev.*, **28**(27–28), 3016–3034.
- Keil, R.G., Dickens, A.F., Arnarson, T., Nunn, B.L. and Devol, A.H. (2004) What is the oxygen exposure time of laterally transported organic matter along the Washington margin? *Mar. Chem.*, **92**(1–4), 157–165.
- Kobashi, T., Kawamura, K., Severinghaus, J.P., Barnola, J.M., Nakaegawa, T., Vinther, B.M. and Box, J.E. (2011) High variability of Greenland surface temperature over the past 4000 years estimated from trapped air in an ice core. *Geophys. Res. Lett.*, **38**(21), L21501.
- Korres, G., Ravdas, M., Zacharioudaki, A., Denaxa, D. and Sotiropoulou, M. (2021) *Mediterranean Sea Waves Reanalysis (CMEMS Med-Waves, MedWAM3 system) (Version 1) set*. Copernicus Monitoring Environment Marine Service (CMEMS).
- Lamb, M.P., Myrow, P.M., Lukens, C., Houck, K. and Strauss, J. (2008) Deposits from wave-influenced turbidity currents: Pennsylvanian Minturn Formation, Colorado, USA. *J. Sediment. Res.*, **78**(7), 480–498.
- Laycock, D.P., Pedersen, P.K., Montgomery, B.C. and Spencer, R.J. (2017) Identification, characterization, and statistical analysis of mudstone aggregate clasts, Cretaceous Carlile Formation, Central Alberta, Canada. *Mar. Petrol. Geol.*, **84**, 49–63.
- Lazar, O.R., Bohacs, K.M., Macquaker, J.H., Schieber, J. and Demko, T.M. (2015a) Capturing key attributes of fine-grained sedimentary rocks in outcrops, cores, and thin sections: nomenclature and description guidelines. *J. Sed. Res.*, **85**(3), 230–246.

- Lazar, O.R., Bohacs, K.M., Schieber, J., Macquaker, J.H.S. and Demko, T.M. (2015b) *Mudstone primer: Lithofacies Variations, Diagnostic Criteria, and Sedimentologic-Stratigraphic Implications at lamina to Bedset Scale*. SEPM (Society for Sedimentary Geology), 205 pp.
- Leonowicz, P.M. (2013) The significance of mudstone fabric combined with palaeoecological evidence in determining sedimentary processes-an example from Middle Jurassic of southern Poland. *Geol. Q.*, **57**(2), 243–260.
- Li, Z. and Schieber, J. (2018) Composite Particles in Mudstones: Examples from the Late Cretaceous Tununk Shale Member of the Mancos Shale Formation. *J. Sed. Res.*, **88**(12), 1319–1344.
- Li, Z. and Schieber, J. (2022) Correlative conformity or subtle unconformity? The distal expression of a sequence boundary in the Upper Cretaceous Mancos Shale, Henry Mountains Region, Utah, USA. *J. Sediment. Res.*, **92**(7), 635–657.
- Li, Z., Bhattacharya, J. and Schieber, J. (2015) Evaluating along-strike variation using thin-bedded facies analysis, Upper Cretaceous Ferron Notom Delta, Utah. *Sedimentology*, **62**, 2060–2089.
- Li, Z., Schieber, J. and Pedersen, P.K. (2021) On the origin and significance of composite particles in mudstones: Examples from the Cenomanian Dunvegan Formation. *Sedimentology*, **68**(2), 737–754.
- Liu, J.P., Li, A.C., Xu, K.H., Velozzi, D.M., Yang, Z.S., Milliman, J.D. and DeMaster, D.J. (2006) Sedimentary features of the Yangtze River-derived along-shelf clinoform deposit in the East China Sea. *Cont. Shelf Res.*, **26**(17–18), 2141–2156.
- Loucks, R.G. and Ruppel, S.C. (2007) Mississippian Barnett Shale: Lithofacies and depositional setting of a deep-water shale-gas succession in the Fort Worth Basin, Texas. *AAPG Bull.*, **91**(4), 579–601.
- Lovell, J.P.B. and Stow, D.A.V. (1981) Identification of ancient sandy contourites. *Geology*, **9**(8), 347–349.
- Macquaker, J.H.S., Bentley, S.J. and Bohacs, K.M. (2010) Wave-enhanced sediment-gravity flows and mud dispersal across continental shelves: Reappraising sediment transport processes operating in ancient mudstone successions. *Geology*, **38**(10), 947–950.
- Mancinelli, A. (2000) Studi, indagini e modelli matematici finalizzati alla redazione del piano di difesa della costa. F Trasporto solido fluviale e dinamica delle foci, Regione Marche, Servizio Lavori Pubblici, Ufficio Progetti, 1–25.
- Marini, M., Maselli, V., Campanelli, A., Foglini, F. and Grilli, F. (2016) Role of the Mid-Adriatic deep in dense water interception and modification. *Mar. Geol.*, **375**, 5–14.
- Martin, P.J., Book, J.W., Burrage, D.M., Rowley, C.D. and Tudor, M. (2009) Comparison of model-simulated and observed currents in the central Adriatic during DART. *J. Geophys. Res. Oceans*, **114**(C2), 4842.
- Martín-Chivelet, J., Fregenal-Martínez, M.A. and Chacón, B. (2008) Traction structures in contourites. *Dev. Sedimentol.*, **60**, 157–182.
- Maselli, V. and Trincardi, F. (2013) Man made deltas. *Sci. Rep.*, **3**, 1926.
- Matthes, F.E. (1939) Report of committee on glaciers, April 1939. *Eos, Transac. Am. Geophys. Union*, **20**(4), 518–523.
- McDermott, F., Matthey, D.P. and Hawkesworth, C. (2001) Centennial-scale Holocene climate variability revealed by a high-resolution speleothem $\delta^{18}\text{O}$ record from SW Ireland. *Science*, **294**, 1329–1331.
- Mellere, D., Plink-Björklund, P. and Steel, R. (2002) Anatomy of shelf deltas at the edge of a prograding Eocene shelf margin, Spitsbergen. *Sedimentology*, **49**(6), 1181–1206.
- Milker, Y. and Schmiedl, G. (2012) A taxonomic guide to modern benthic shelf foraminifera of the western Mediterranean Sea. *Palaeontol. Electron.*, **15**, 134.
- Milliman, J.D. and Syvitski, J.P.M. (1992) Geomorphic/tectonic control of sediment discharge to the ocean: the importance of small mountainous rivers. *J. Geol.*, **100**, 525–544.
- Minisini, D., Eldrett, J., Bergman, S.C. and Forkner, R. (2018) Chronostratigraphic framework and depositional environments in the organic-rich, mudstone-dominated Eagle Ford Group, Texas, USA. *Sedimentology*, **65**, 1520–1557.
- Miramontes, E., Eggenhuisen, J.T., Jacinto, R.S., Poneti, G., Pohl, F., Normandeau, A. and Hernández-Molina, F.J. (2020) Channel-levee evolution in combined contour current-turbidity current flows from flume-tank experiments. *Geology*, **48**(4), 353–357.
- Morehead, M.D., Syvitski, J.P., Hutton, E.W. and Peckham, S.D. (2003) Modeling the temporal variability in the flux of sediment from ungauged river basins. *Global Planet. Change*, **39**, 95–110.
- Morris, V., Clemente-Colón, P., Nalli, N.R., Joseph, E., Armstrong, R.A., Detrés, Y., Goldbred, M.D., Minnett, P.J. and Lumpkin, R. (2006) Measuring trans-Atlantic aerosol transport from Africa. *Eos*, **87**(50), 565–571.
- Morsilli, M., Bosellini, A. and Rusciadelli, G. (2004) The Apulia carbonate platform margin and slope, Late Jurassic to Eocene of the Maiella and Gargano Promontory: Physical stratigraphy and architecture. In: *32nd International Geological Congress* (Ed. APAT Roma), pp. 1–44. APAT Roma, Florence.
- Morucci, S., Picone, M., Nardone, G. and Arena, G. (2016) Tides and waves in the Central Mediterranean Sea. *J. Oper. Oceanogr.*, **9**(sup1), s10–s17.
- Mulder, T. and Syvitski, J.P.M. (1995) Turbidity currents generated at river mouths during exceptional discharge to the world's oceans. *J. Geol.*, **103**, 285–298.
- Mulder, T., Syvitski, J.P., Migeon, S., Faugères, J.C. and Savoye, B. (2003) Marine hyperpycnal flows: initiation, behavior and related deposits. A review. *Mar. Petrol. Geol.*, **20**, 861–882.
- Mulder, T., Faugères, J.C. and Gonthier, E. (2008) Mixed turbidite-contourite systems. *Dev. Sedimentol.*, **60**, 435–456.
- Mutti, E., Tinterri, R., Benevelli, G., di Biase, D. and Cavanna, G. (2003) Deltaic, mixed and turbidite sedimentation of ancient foreland basins. *Mar. Petrol. Geol.*, **20**(6–8), 733–755.
- Myrow, P.M., Fischer, W. and Goodge, J.W. (2002) Wave-modified turbidites: combined-flow shoreline and shelf deposits, Cambrian, Antarctica. *J. Sed. Res.*, **72**(5), 641–656.
- Myrow, P.M., Lukens, C., Lamb, M.P., Houck, K. and Strauss, J. (2008) Dynamics of a transgressive prodeltaic system: Implications for geography and climate within a Pennsylvanian intracratonic basin, Colorado, USA. *J. Sed. Res.*, **78**, 512–528.
- Nittrouer, C.A., Kuehl, S.A., DeMaster, D.J. and Kowsmann, R.O. (1986) The deltaic nature of Amazon shelf sedimentation. *Geol. Soc. Am. Bull.*, **97**(4), 444–458.
- Normark, W.R. and Piper, D.J. (1991) Initiation processes and flow evolution of turbidity currents: implications for the depositional record. In: *From Shoreline to Abyss*:

- Contributions in Marine Geology in Honor of Francis Parker Shepard* (Ed. Osborne, R.H.), *SEPM Spec. Publ.*, **46**, 320.
- Nummedal, D. and Swift, D.J. (1987) Transgressive stratigraphy at sequence-bounding unconformities: some principles derived from Holocene and Cretaceous examples. *SEPM Spec. Publ.*, **41**, 241.
- Nyhuys, C.J., Riley, D. and Kalasinska, A. (2014) Thin section petrography and chemostratigraphy: Integrated evaluation of an upper Mississippian mudstone dominated succession from the southern Netherlands. *Neth. J. Geosci.*, **95**, 3–22.
- O'Brien, N.R. (1996) Shale lamination and sedimentary processes. *Geol. Soc. Spec. Publ.*, **116**(1), 23–36.
- Ogston, A.S., Sternberg, R.W., Nittrouer, C.A., Martin, D.P., Goñi, M.A. and Crockett, J.S. (2008) Sediment delivery from the Fly River tidally dominated delta to the nearshore marine environment and the impact of El Niño. *J. Geophys. Res. Earth Surf.*, **113**(F1), 669.
- Olariu, C. and Bhattacharya, J.P. (2006) Terminal distributary channels and delta front architecture of river-dominated delta systems. *J. Sed. Res.*, **76**, 212–233.
- Olariu, C., Steel, R.J. and Petter, A.L. (2010) Delta-front hyperpycnal bed geometry and implications for reservoir modeling: Cretaceous Panther Tongue delta, Book Cliffs, Utah. *AAPG Bull.*, **94**(6), 819–845.
- Oldfield, F., Asoli, A., Accorsi, C.A., Mercuri, A.M., Juggins, S., Langone, L., Rolph, T., Trincardi, F., Wolff, G., Gibbs, Z., Vigliotti, L., Frignani, M., van der Post, K. and Branch, N. (2003) A high resolution late Holocene palaeo environmental record from the central Adriatic Sea. *Quatern. Sci. Rev.*, **22**, 319–342.
- Palinkas, C.M. (2009) The timing of floods and storms as a controlling mechanism for shelf deposit morphology. *J. Coastal Res.*, **25**(5), 1122–1129.
- Palinkas, C.M. and Nittrouer, C.A. (2006) Clinoform sedimentation along the Apennine shelf, Adriatic Sea. *Mar. Geol.*, **234**(1–4), 245–260.
- Parsons, J.D., Bush, J.W. and Syvitski, J.P. (2001) Hyperpycnal plume formation from riverine outflows with small sediment concentrations. *Sedimentology*, **48**, 465–478.
- Patruno, S., Hampson, G.J. and Jackson, C.A. (2015) Quantitative characterisation of deltaic and subaqueous clinoforms. *Earth-Sci. Rev.*, **142**, 79–119.
- Patruno, S. and Helland-Hansen, W. (2018) Clinoforms and clinoform systems: Review and dynamic classification scheme for shorelines, subaqueous deltas, shelf edges and continental margins. *Earth-Sci. Rev.*, **185**, 202–233.
- Paz, M., Buatois, L.A., Mángano, M.G., Desjardins, P.R., Notta, R., Tomassini, F.G., Carmona, N.B. and Minisini, D. (2022) Organic-rich, fine-grained contourites in an epicontinental basin: The Upper Jurassic-Lower Cretaceous Vaca Muerta Formation, Argentina. *Mar. Petrol. Geol.*, **142**, 105757.
- Pellegrini, C., Maselli, V., Cattaneo, A., Piva, A., Ceregato, A. and Trincardi, F. (2015) Anatomy of a compound delta from the post-glacial transgressive record in the Adriatic Sea. *Mar. Geol.*, **362**, 43–59.
- Pellegrini, C., Maselli, V., Gamberi, F., Asoli, A., Bohacs, K.M., Drexler, T.M. and Trincardi, F. (2017) How to make a 350-m-thick lowstand systems tract in 17,000 years: The Late Pleistocene Po River (Italy) lowstand wedge. *Geology*, **45**(4), 327–330.
- Pellegrini, C., Asoli, A., Bohacs, K.M., Drexler, T.M., Feldman, H.R., Sweet, M.L. and Trincardi, F. (2018) The late Pleistocene Po River lowstand wedge in the Adriatic Sea: Controls on architecture variability and sediment partitioning. *Mar. Petrol. Geol.*, **96**, 16–50.
- Pellegrini, C., Patruno, S., Helland-Hansen, W., Steel, R.J. and Trincardi, F. (2020) Clinoforms and clinothems: Fundamental elements of basin infill. *Basin Res.*, **32**(2), 187–205.
- Pellegrini, C., Tesi, T., Schieber, J., Bohacs, K.M., Rovere, M., Asoli, A., Nogarotto, A. and Trincardi, F. (2021) Fate of terrigenous organic carbon in muddy clinothems on continental shelves revealed by stratal geometries: Insight from the Adriatic sedimentary archive. *Global Planet. Change*, **203**, 103539.
- Peng, Y., Yu, Q., Du, Z., Wang, L., Wang, Y. and Gao, S. (2022) Gravity-driven sediment flows on the shallow sea floor of a muddy open coast. *Mar. Geol.*, **445**, 106759.
- Petter, A.L. (2010) *Stratigraphic Implications of the Spatial and Temporal Variability in Sediment Transport in Rivers, Deltas, and Shelf Margins*. The University of Texas at Austin, Austin, TX.
- Piva, A., Asoli, A., Trincardi, F., Schneider, R.R. and Vigliotti, L. (2008) Late-Holocene climate variability in the Adriatic Sea (Central Mediterranean). *Holocene*, **18**(1), 153–167.
- Plint, A.G. (2014) Mud dispersal across a Cretaceous prodelta: storm-generated, wave-enhanced sediment gravity flows inferred from mudstone microtexture and microfacies. *Sedimentology*, **61**(3), 609–647.
- Potter, P.E., Maynard, J.B. and Pryor, W.A. (2012) *Sedimentology of Shale: Study Guide and Reference Source*. Springer, New York.
- Poulain, P.M. (2001) Adriatic Sea surface circulation as derived from drifter data between 1990 and 1999. *J. Mar. Syst.*, **29**(1–4), 3–32.
- Poulain, P.M. (2013) Tidal currents in the Adriatic as measured by surface drifters. *J. Geophys. Res.*, **118**(3), 1434–1444.
- Poyatos-Moré, M., Jones, G.D., Brunt, R.L., Hodgson, D.M., Wild, R.J. and Flint, S.S. (2016) Mud-dominated basin-margin progradation: processes and implications. *J. Sed. Res.*, **86**(8), 863–878.
- Poyatos-Moré, M., Jones, G.D., Brunt, R.L., Tek, D.E., Hodgson, D.M. and Flint, S.S. (2019) Clinoform architecture and along-strike facies variability through an exhumed erosional to accretionary basin margin transition. *Basin. Res.*, **31**(5), 920–994.
- Pratt, L.M. (1984) Influence of paleoenvironmental factors on preservation of organic matter in Middle Cretaceous Greenhorn Formation, Pueblo, Colorado. *AAPG Bull.*, **68** (9), 1146–1159.
- Puig, P., Ogston, A.S., Guillén, J., Fain, A.M.V. and Palanques, A. (2007) Sediment transport processes from the topset to the foreset of a crenulated clinoform (Adriatic Sea). *Continental Shelf Res.*, **27**(3–4), 452–474.
- Reading, H.G. (2001) Clastic facies models, a personal perspective. *Bull. Geol. Soc. Denmark*, **48**, 101–115.
- Renaud, F.G., Syvitski, J.P., Sebesvari, Z., Werners, S.E., Kremer, H., Kuenzer, C. and Friedrich, J. (2013) Tipping from the Holocene to the Anthropocene: how threatened are major world deltas? *COSUST*, **5**(6), 644–654.
- Rice, A.E., Book, J.W., Carniel, S., Russo, A., Schroeder, K. and Wood, W.T. (2013) Spring 2009 water mass distribution, mixing and transport in the southern Adriatic after a low production of winter dense waters. *Cont. Shelf Res.*, **64**, 33–50.

- Rittersbacher, A., Howell, J.A. and Buckley, S.J.** (2014) Analysis of fluvial architecture in the Blackhawk Formation, Wasatch Plateau, Utah, USA, using large 3D photorealistic models. *J. Sed. Res.*, **84**, 72–87.
- Rodriguez, A.B., Anderson, J.B., Siringan, F.P. and Taviani, M.** (2004) Holocene evolution of the east Texas coast and inner continental shelf: along-strike variability in coastal retreat rates. *J. Sed. Res.*, **74**, 405–421.
- Rossi, V. and Vaiani, S.C.** (2008) Benthic foraminiferal evidence of sediment supply changes and fluvial drainage reorganization in Holocene deposits of the Po Delta, Italy. *Mar. Micropaleontol.*, **69**(2), 106–118.
- Rossi, V.M., Perillo, M.M., Steel, R.J. and Olariu, C.** (2017) Quantifying mixed-process variability in shallow-marine depositional systems: What are sedimentary structures really telling us? *Journal of Sedimentary Research*, **87**(10), 1060–1074.
- Rossi, V., Barbieri, G., Vaiani, S.C. and Amorosi, A.** (2021) Benthic foraminifers from Holocene subaqueous deltas of the Western Mediterranean: Stratigraphic implications and palaeoenvironmental significance of the biofacies. *Mar. Geol.*, **442**, 106632.
- Rothwell, R.G. and Rack, F.R.** (2006) New techniques in sediment core analysis: an introduction. *Geol. Soc. Spec. Publ.*, **267**(1), 1–29.
- Rovere, M., Pellegrini, C., Chiggiato, J., Campiani, E. and Trincardi, F.** (2019) Impact of dense bottom water on a continental shelf: An example from the SW Adriatic margin. *Mar. Geol.*, **408**, 123–143.
- Schieber, J.** (1998) Deposition of mudstones and shales: Overview, problems, and challenges. In: *Shales and Mudstones: Basin Studies, Sedimentology and Paleontology*, Vol. 1, pp. 131–146. Schweizerbart'sche Verlagsbuchhandlung, Stuttgart.
- Schieber, J.** (1999) Distribution and deposition of mudstone facies in the upper Devonian Sonyea Group of New York. *J. Sed. Res.*, **69**, 909–925.
- Schieber, J.** (2002) The Role of an Organic Slime Matrix in the Formation of Pyritized Burrow Trails and Pyrite Concretions. *Palaios*, **17**, 104–109.
- Schieber, J.** (2011) Reverse engineering mother nature—Shale sedimentology from an experimental perspective. *Sed. Geol.*, **238**(1–2), 1–22.
- Schieber, J.** (2016) Mud re-distribution in epicontinental basins—exploring likely processes. *Mar. Petrol. Geol.*, **71**, 119–133.
- Schieber, J. and Shao, X.** (2021) Detecting detrital carbonate in shale successions – Relevance for evaluation of depositional setting and sequence stratigraphic interpretation. *Mar. Petrol. Geol.*, **130**, 105130.
- Schieber, J. and Southard, J.B.** (2009) Bedload transport of mud by floccule ripples – direct observation of ripple migration processes and their implications. *Geology*, **37**, 483–486.
- Schieber, J. and Yawar, Z.** (2009) A new twist on mud deposition – mud ripples in experiment and rock record. *Sediment. Rec.*, **7**(2), 4–8.
- Schieber, J., Krinsley, D. and Riciputi, L.** (2000) Diagenetic origin of quartz silt in mudstones and implications for silica cycling. *Nature*, **406**(6799), 981–985.
- Schieber, J., Southard, J.B. and Thaisen, K.G.** (2007) Accretion of mudstone beds from migrating floccule ripples. *Science*, **318**(5857), 1760–1763.
- Schieber, J., Southard, J.B. and Schimmelmann, A.** (2010) Lenticular shale fabrics resulting from intermittent erosion of muddy sediments – comparing observations from flume experiments to the rock record. *J. Sediment. Res.*, **80**, 119–128.
- Schieber, J., Miclăuș, C., Seserman, A., Liu, B. and Teng, J.** (2019) When a mudstone was actually a “sand”: Results of a sedimentological investigation of the bituminous marl formation (Oligocene), Eastern Carpathians of Romania. *Sed. Geol.*, **384**, 12–28.
- Schimmelmann, A., Riese, D.J. and Schieber, J.** (2015) Fast and economical sampling and resin-embedding technique for small cores of unconsolidated, fine-grained sediment, 2015 Pacific Climate (PACCLIM) Workshop, 8–11 March, Asilomar Conference Grounds, Pacific Grove, California, pp. 50–51. (abstracts).
- Schwarz, E., Veiga, G.D., Álvarez Trentini, G., Isla, M.F. and Spalletti, L.A.** (2018) Expanding the spectrum of shallow-marine, mixed carbonate–siliciclastic systems: Processes, facies distribution and depositional controls of a siliciclastic-dominated example. *Sedimentology*, **65**(5), 1558–1589.
- Schwarz, E., Poyatos-Moré, M., Boya, S., Gomis-Cartesio, L. and Midtkandal, I.** (2021) Architecture and controls of thick, intensely bioturbated, storm-influenced shallow-marine successions: An example from the Jurassic Neuquén Basin (Argentina). *Palaeogeogr. Palaeoclimatol. Palaeoecol.*, **562**, 110109.
- Sellschopp, J. and Álvarez, A.** (2003) Dense low-salinity outflow from the Adriatic Sea under mild (2001) and strong (1999) winter conditions. *J. Geophys. Res. Oceans*, **108**(C9), 1562.
- Sgarrella, F. and Moncharmont Zei, M.** (1993) Benthic foraminifera of the Gulf of Naples (Italy): systematics and autoecology. *Boll. Soc. Paleontol. Ital.*, **32**, 145–264.
- Shanmugam, G.** (2000) 50 years of the turbidite paradigm (1950s–1990s): deep-water processes and facies models—a critical perspective. *Mar. Pet. Geol.*, **17**(2), 285–342.
- Shanmugam, G., Spalding, T.D. and Rofheart, D.H.** (1993) Traction structures in deep-marine, bottom-current-reworked sands in the Pliocene and Pleistocene, Gulf of Mexico. *Geology*, **21**(10), 929–932.
- Singh, P., Slatt, R. and Coffey, W.** (2008) Barnett Shale – unfolded: sedimentology, sequence stratigraphy, and regional mapping. *Gulf Coast Assoc. Geol. Soc. Trans.*, **58**, 777–795.
- Slootman, A. and Cartigny, M.J.** (2020) Cyclic steps: review and aggradation-based classification. *Earth-Sci. Rev.*, **201**, 102949.
- Sømme, T.O., Piper, D.J., Deptuck, M.E. and Helland-Hansen, W.** (2011) Linking onshore-offshore sediment dispersal in the Golo source-to-sink system (Corsica, France) during the late Quaternary. *J. Sed. Res.*, **81**(2), 118–137.
- Sorrel, P., Debret, M., Billeaud, I., Jaccard, S.L., McManus, J.F. and Tessier, B.** (2012) Persistent non-solar forcing of Holocene storm dynamics in coastal sedimentary archives. *Nat. Geosci.*, **5**(12), 892–896.
- Stow, D.A. and Shanmugam, G.** (1980) Sequence of structures in fine-grained turbidites: comparison of recent deep-sea and ancient flysch sediments. *Sed. Geol.*, **25**(1–2), 23–42.
- Stow, D. and Smillie, Z.** (2020) Distinguishing between deep-water sediment facies: Turbidites, contourites and hemipelagites. *Geosciences*, **10**(2), 68.
- Stow, D.A., Bishop, C.D. and Mills, S.J.** (1982) Sedimentology of the Brae oilfield, North Sea: fan models and controls. *J. Pet. Geol.*, **5**(2), 129–148.

- Stow, D.A., Faugères, J.C., Viana, A. and Gonthier, E. (1998) Fossil contourites: a critical review. *Sed. Geol.*, **115**(1-4), 3–31.
- Syvitski, J.P., Morehead, M.D., Bahr, D.B. and Mulder, T. (2000) Estimating fluvial sediment transport: the rating parameters. *Water Resour. Res.*, **36**(9), 2747–2760.
- Talling, P.J., Masson, D.G., Sumner, E.J. and Malgesini, G. (2012) Subaqueous sediment density flows: Depositional processes and deposit types. *Sedimentology*, **59**, 1937–2003.
- Taylor, A.M. and Goldring, R. (1993) Description and analysis of bioturbation and ichnofabric. *J. Geol. Soc.*, **150** (1), 141–148.
- Tentori, D., Amorosi, A., Milli, S. and Marsaglia, K.M. (2021) Sediment dispersal pathways in the Po coastal plain since the Last Glacial Maximum: Provenance signals of autogenic and eustatic forcing. *Basin Res.*, **33**, 1407–1428.
- Tesi, T., Miserocchi, S., Goñi, M.A. and Langone, L. (2007) Source, transport and fate of terrestrial organic carbon on the western Mediterranean Sea, Gulf of Lions, France. *Mar. Chem.*, **105**, 101–117.
- Thöle, L.M., Amsler, H.E., Moretti, S., Auderset, A., Gilgannon, J., Lippold, J., Vogel, H., Crosta, X., Mazaud, A., Michel, E., Martínez-García, A. and Jaccard, S.L. (2019) Glacial-interglacial dust and export production records from the Southern Indian Ocean. *Earth Planet. Sci. Lett.*, **525**, 115716.
- Trabucho-Alexandre, J., Dirkx, R., Veld, H., Klaver, G. and de Boer, P.L. (2012) Toarcian black shales in the Dutch Central Graben: record of energetic, variable depositional conditions during an oceanic anoxic event. *J. Sed. Res.*, **82** (2), 104–120.
- Traykovski, P., Wiberg, P.L. and Geyer, W.R. (2007) Observations and modeling of wave-supported sediment gravity flows on the Po prodelta and comparison to prior observations from the Eel shelf. *Cont. Shelf Res.*, **27**(3-4), 375–399.
- Trincardi, F., Campiani, E., Correggiari, A., Foglini, F., Maselli, V. and Remia, A. (2014) Bathymetry of the Adriatic Sea: The legacy of the last eustatic cycle and the impact of modern sediment dispersal. *J. Maps*, **10**(1), 151–158.
- Van der Zwaan, G.J. and Jorissen, F.J. (1991) Biofacial patterns in river-induced shelf anoxia. *Geol. Soc. Spec. Publ.*, **58**(1), 65–82.
- Van Wagoner, J.C. (1995) Overview of sequence stratigraphy of foreland basin deposits: terminology, summary of papers, and glossary of sequence stratigraphy. In: *Sequence Stratigraphy of Foreland Basin Deposits* (Eds Van Wagoner, J.C. and Bertram, G.T.). The American Association of Petroleum Geologists, Tulsa, OK.
- Van Wagoner, J.C., Posamentier, H.W., Mitchum, R.M.J., Vail, P.R., Sarg, J.F., Loutit, T.S. and Hardenbol, J. (1988) An overview of sequence stratigraphy and key definitions. In: *Sea Level Changes—An Integrated Approach* (Eds Wilgus, C.K., Hastings, B.S., Kendall, C.G.St.C., Posamentier, H.W., Ross, C.A. and Van Wagoner, J.C.), *SEPM Spec. Publ.*, **42**, 39–45.
- Van Wagoner, J.C., Mitchum, R.M., Campion, K.M. and Rahmanian, V.D. (1990) *Siliciclastic sequence stratigraphy in well logs, cores, and outcrops: concepts for high-resolution correlation of time and facies*. American Association of Petroleum Geologists, Tulsa, OK.
- Walsh, J.P. and Nittrouer, C.A. (2009) Understanding fine-grained river-sediment dispersal on continental margins. *Mar. Geol.*, **263**(1-4), 34–45.
- Walsh, J.P., Corbett, D.R., Kiker, J.M., Orpin, A.R., Hale, R.P. and Ogston, A.S. (2014) Spatial and temporal variability in sediment deposition and seabed character on the Waipaoa River margin, New Zealand. *Cont. Shelf Res.*, **86**, 85–102.
- Wang, X.H. and Pinardi, N. (2002) Modeling the dynamics of sediment transport and resuspension in the northern Adriatic Sea. *J. Geophys. Res. Oceans*, **107**(C12), 11–18.
- Weltje, G.J. and Tjallingii, R. (2008) Calibration of XRF core scanners for quantitative geochemical logging of sediment cores: Theory and application. *Earth Planet. Sci. Lett.*, **274** (3-4), 423–438.
- Wheatcroft, R.A., Stevens, A.W., Hunt, L.M. and Milligan, T.G. (2006) The large-scale distribution and internal geometry of the fall 2000 Po River flood deposit: evidence from digital X-radiography. *Cont. Shelf Res.*, **26**(4), 499–516.
- Wilson, R.D. and Schieber, J. (2014) Muddy hyperpycnites in the Lower Genesee Group of Central New York, USA: implications for mud transport in epicontinental seas. *J. Sed. Res.*, **84**, 866–874.
- Yawar, Z. and Schieber, J. (2017) On the origin of silt laminae in laminated shales. *Sed. Geol.*, **360**, 22–34.
- Yu, X., Stow, D., Smillie, Z., Esentia, I., Brackenridge, R., Xie, X., Bankole, S., Ducassou, E. and Llave, E. (2020) Contourite porosity, grain size and reservoir characteristics. *Mar. Petr. Geol.*, **117**, 104392.
- Zavala, C., Arcuri, M., Di Meglio, M., Gamero Diaz, H. and Contreras, C. (2011) A genetic facies tract for the analysis of sustained hyperpycnal flow deposits. In: *Sediment transfer from shelf to deep water—Revisiting the delivery system* (Eds. R.M. Slatt and C. Zavala). *AAPG Studies Geol.*, **61**, 31–51.
- Zonneveld, K.A.F., Versteegh, G.J.M., Kasten, S., Eglinton, T.I., Emeis, K.C., Huguet, C., Koch, B.P., de Lange, G.L., de Leeuw, J.W., Middelburg, J.J., Mollenhauer, G., Prahl, G.H., Rethemeyer, J. and Wakeham, S.G. (2010) Selective preservation of organic matter in marine environments: processes and impact on the sedimentary record. *Biogeosciences*, **7**(2), 483–511.

Manuscript received 19 February 2023; revision accepted 4 November 2023

Supporting Information

Additional information may be found in the online version of this article:

Fig S1. Relative abundances of the main ostracod and foraminiferal taxa plotted against stratigraphy of the studied cores (KS02-219, KS02-357 and AMC99-09).

Table S1. Absolute abundances of ostracod and foraminiferal taxa from core samples (KS02-219, KS02-357 and AMC99-09).

Table S2. Ecological Categories (ECs) for the ostracod and foraminiferal taxa encountered within the studied cores (KS02-219, KS02-357 and AMC99-09).

Table S3. Relative abundances of the main ostracod and foraminiferal taxa plotted against stratigraphy of the studied cores (KS02-219, KS02-357 and AMC99-09).